Response to Anonymous Referee #1's comments on "Analyses of Uncertainties and Scaling of Groundwater Level Fluctuations"

General comments: *This paper deals with uncertainties in groundwater level in unconfined aquifers due to temporal variations of hydrological processes. It derives the head covariance function for 1-D transient flow in a bounded unconfined aquifer with random recharge as well as random initial and boundary conditions. Associated time-dependent spectral densities are also derived, allowing to investigate the existence of temporal scaling of groundwater level fluctuations. The topic of the note lies within the aims and scope of Hydrology and Earth System Sciences and is a valuable addition to the existing literature. The paper is well-written and concise, and deals with a topic of considerable interest. The mathematical derivations are accurate.*

Response: Thank you for the reviewer's positive comment on our study.

Specific comments: *Specific suggestions to improve the quality of the paper are listed below.*

1. *The authors should mention specific applications of their results to real cases, to help the paper convey a take-home message.*
   Response: This is an excellent comment. The analytical solutions for the head variances derived in this study provide a way to quantify the uncertainty in the groundwater levels calculated with analytical and numerical solutions with uncertain recharge, source/sink, and boundary conditions. The spectrum relationship among the head, recharge and boundary conditions obtained in this study can help one to improve spectrum analysis for a groundwater level time series and to remove the erects of boundary conditions. Specific applications of the results obtained in this study are to help one to identify and quantify the sources of uncertainties in the system he/she studied. We added these in lines 375-379 of the revised manuscript.

2. *I suggest to add a schematic of the system investigated for the sake of clarity. This will help clarifying the meaning of the quantity M, defined at line 152 as the average saturated thickness of the aquifer. Since h is random, M should incorporate an element of randomness.*
   Response: As suggested by the reviewer, we added a schematic of the system studied, i.e., the new Figure 1 in the revised manuscript. Please note that it is assumed in this study that the fluctuation of the head is relatively small as compared to the aquifer thickness and the unconfined flow equation was linearized and thus the average saturated thickness of the aquifer (M) was assumed to be constant.

3. *A key assumption in the analysis is that W(t), Q(t), and H(t) are uncorrelated (see line 137). Given the geometrical setup, this assumption is not warranted. The paper could benefit from discussing this issue, and, specifically, realistic conditions for the validity of the assumption.*
   Response: This is again an excellent comment. In general, W(t), Q(t), and H(t) should be correlated. It is possible to consider the relationship among W(t), Q(t), and H(t) by assuming some theoretical correlation functions but the problem is that 1) it is unclear

what kind of correlation exists among these variable, 2) there is little observed or measured data to support any type of the correlation assumed, and 3) simple analytical solutions would be difficulty to derive when considering such a correlation. Therefore, we studied the case in which such correlation is weak or no correlation in order to derive some simple analytical solutions. We believe this is an important first step towards solving this complex problem and more research in needed in this direction, especially about the correlation among the recharge, flux, and boundary conditions. We hope to relax this assumption in our future study.

4. *(a) Temporal scaling of groundwater level fluctuations is shown to exist at intermediate and late times, and to be dominated by the effect of random recharge as opposed to that of random boundary conditions. Why? Is this valid only for the specific parameters examined? (b) When spectra associated with one random effect at a time are examined, different scalings (1/f, 1/f^2) are found. Why does this happen?*

   Response:

   a) We think the reason that the temporal scaling of groundwater level is dominated by the random recharge is that the areal recharge occurs over entire the aquifer and thus affect the groundwater level everywhere in the aquifer while the boundary conditions affect a relatively small area near the boundaries in most aquifers. The specific parameters used in this study are typical for a real aquifer. The effect of the boundary conditions or the area of the influence by the boundary conditions would be enhanced in a more permeable aquifer. However, in most aquifers areal recharge should be the dominating force affecting groundwater level fluctuations and its scaling.

   b) We do not totally understand this comment. That the groundwater level fluctuates as a $1/f$ noise only at $x'=0$ under the random flux boundary, and it fluctuates as a $1/f^2$ noise at most locations only under random recharge when the characteristic time scale (t_c) is large, i.e., $t_c > 400$ days .

Minor points:

1. *Check keywords.*

   Response: We revised the keywords as: Uncertainty of groundwater levels; Temporal scaling; Random source/sink; Random initial and boundary conditions.

2. *Check line 75.*

   Response: We checked but didn't find any problem in this line.

3. *Check equation (12).*

   Response: We checked the Eq. (12) in our original submission (now is Eq. 11 in the revision) and didn't find any error. However, there are two typos in Eq. (8) and (9): one is that the Eqs. (8) and (9) are actually one equation, and the other is in the first term on the right hand of the equation. We corrected these typos. The correct Eq. (8) was given in the revision.

4. *Check Line 173, 'is' is missing.*
   Response: We added it.

5. *Line 175, in 'decay' a 's' is missing.*
   Response: We added it.

6. Line 204, check if 'the' is missing.
   Response: We added "the " before "most aquifers".

7. Line 223, check if 'on' is missing.
   Response: We deleted this sentence based on Reviewer #2's comments.

8. Check the sentence at lines 346-347.
   Response: We added 's' after 'curve' and 'location', respectively.

Technical note:

Analyses of Uncertainties and Scaling of Groundwater Level Fluctuations

Xiuyu Liang[a,b] , You-Kuan Zhang[a*,b,c]

[a]Center for Hydrosciences Research, Nanjing University,
Nanjing, Jiangsu 210093, P.R. China

[b]School of Earth Sciences and Engineering, Nanjing University,
Nanjing, Jiangsu 210093, P.R. China

[c]Department of Geoscience, University of Iowa,
Iowa City, Iowa 52242, USA

*Corresponding author
Phone: +86 25-83594485, Fax: +86 25-83596670,
Email: ykzhang@nju.edu.cn

Resubmitted to *Hydrology and Earth System Sciences*
May, 2015

Abstract

Analytical solutions for the variance, covariance, and spectrum of groundwater level, *h(x, t)*, in an unconfined aquifer described by a linearized Boussinesq equation with random source/sink and initial and boundary conditions were derived. It was found that in a typical aquifer the error in *h(x, t)* in early time is mainly caused by the random initial condition and the error reduces as time progresses to reach a constant error in later time. The duration during which the effect of the random initial condition is significant may last a few hundred days in most aquifers. The constant error in *h(x, t)* in later time is due to the combined effects of the uncertainties in the source/sink and flux boundary: the closer to the flux boundary, the larger the error. The error caused by the uncertain head boundary is limited in a narrow zone near the boundary and remains more or less constant over time. The aquifer system behaves as a low-pass filter which filters out high-frequency noises and keeps low-frequency variations. Temporal scaling of groundwater level fluctuations exists in most part of a low permeable aquifer whose horizontal length is much larger than its thickness caused by the temporal fluctuations of areal source/sink.

Key words: Uncertainty of groundwater levels; Temporal scaling; Random source/sink; Random initial and boundary conditions.

1. Introduction

Groundwater level or hydraulic head (h) is the main driving force for water flow and advective contaminant transport in aquifers and thus the most important variable studied in groundwater hydrology and its applications. Knowledge about h is critical in dealing with groundwater-related environmental problems, such as over-pumping, subsidence, sea water intrusion, and contamination. One often found that the data about groundwater level is limited or unavailable in a hydrogeological investigation. In such cases the groundwater level distribution and its temporal variation are usually obtained with an analytical or numerical solution to a groundwater flow model.

It is obvious that errors always exit in the groundwater levels calculated or simulated with analytical or numerical solutions. The main sources of errors include the simplification or approximation in a conceptual model and the uncertainties in the model parameters. Problems in conceptualization or model structure were dealt with by many researchers (Neuman, 2003;Rojas et al., 2010;Ye et al., 2008;Rojas et al., 2008;Refsgaard et al., 2007;Zeng et al., 2013). The uncertainties in the model parameters (e.g., hydraulic conductivity, recharge rate, evapotranspiration, and river conductance) were investigated based on generalized likelihood uncertainty estimation and Bayesian methods (Nowak et al., 2010;Neuman et al., 2012;Rojas et al., 2008;Rojas et al., 2010). The uncertainty in groundwater level has been one of the main research topics in stochastic subsurface hydrology for more than three decades. Most of these studies were focused on the spatial variability of groundwater

63 level due to aquifers' heterogeneity (Dagan, 1989;Gelhar, 1993;Zhang, 2002). Little
64 attention has been given to the uncertainties in groundwater level due to temporal
65 variations of hydrological processes, e.g., recharge, evapotranspiration, discharge to
66 a river, and river stage (Bloomfield and Little, 2010;Zhang and Schilling,
67 2004;Schilling and Zhang, 2012;Liang and Zhang, 2013a;Zhu et al., 2012).

68 Uncertainties of groundwater level fluctuations have been studied by Zhang and
69 Li (2005, 2006) and most recently by Liang and Zhang (2013a). Based on a linear
70 reservoir model with a white noise or temporally-correlated recharge process, Zhang
71 and Li (2005, 2006) derived the variance and covariance of $h(t)$ by considering only
72 a random source or sink process assuming deterministic initial and boundary
73 conditions. Liang and Zhang (2013a) extended the studies of Zhang and Li (2005,
74 2006) and carried out non-stationary spectral analysis and Monte Carlo simulations
75 using a linearized Boussinesq equation, and investigated the temporospatial
76 variations of groundwater level. However, the only random process considered by
77 Liang and Zhang (2013a) is the source/sink. Temporal scaling of groundwater levels
78 discovered first by Zhang and Schilling Zhang and Schilling (2004) was verified in
79 several studies (Zhang and Li, 2005, 2006; Bloomfield and Little, 2010; Zhang and
80 Yang, 2010; Zhu et al., 2012; Schilling and Zhang, 2012). However, we do not know
81 the effect of random boundary conditions on temporal scaling of groundwater levels.

82 In this study we extended above-mentioned work by considering the
83 groundwater flow in a bounded aquifer described by a linearized Boussinesq
84 equation with a random source/sink as well as random initial and boundary

conditions since the latter processes are known with uncertainties. The objectives of this study are 1) to derive analytical solutions for the covariance, variance and spectrum of groundwater level, and 2) to investigate the individual and combined effects of these random processes on uncertainties and scaling of *h(x, t)*. In the following we will first present the formulation and analytical solutions, then discuss the results, and finally draw some conclusions.

2. Formulation and Solutions

Under the Dupuit assumption, the one-dimensional transient groundwater flow in an unconfined aquifer near a river (Fig. 1) can be approximated with the linearized Boussinesq equation (Bear, 1972) with the initial and boundary conditions, i.e.,

$$T\frac{\partial^2 h}{\partial x^2}+W(t)=S_Y\frac{\partial h}{\partial t} \qquad (1a)$$

$$h(x,t)_{|t=0}=H_0(x); \qquad T\frac{\partial h}{\partial x}\bigg|_{x=0}=Q(t); \qquad h(x,t)\big|_{x=L}=H(t) \qquad (1b)$$

where T [L/T] is the transmissivity, h [L] is the hydraulic head or groundwater level above the bottom of the aquifer which is assumed to be horizontal, $W(t)$ [L/T] is the time-dependent source/sink term representing areal recharge or evapotranspiration, S_Y is the specific yield, $H_0(x)$ [L] is the initial condition, $Q(t)$ [L^2/T] is the time-dependent flux at the left boundary, $H(t)$ [L] is the time-dependent water level at the right boundary, L [L] is distance from the left to the right boundary, x [L] is the coordinate, and t [T] is time. In this study the initial head $H_0(x)$ is taken to be a spatially random variable, and the source/sink, $W(t)$, the flux to the left boundary, $Q(t)$, and the head at the right boundary, $H(t)$, are all taken to be temporally random

processes and spatially deterministic. The parameters T and S_Y are taken to be constant.

The groundwater level, *h(x, t),* the three random processes, *W(t), Q(t),* and *H(t),* and the random variable, $H_0(x)$, are expressed in terms of their respective ensemble means plus small perturbations,

$$h(x,t) = \langle h(x,t) \rangle + h'(x,t) \tag{2a}$$

$$W(t) = \langle W(t) \rangle + W'(t); \qquad Q(t) = \langle Q(t) \rangle + Q'(t) \tag{2b}$$

$$H(t) = \langle H(t) \rangle + H'(t); \qquad H_0(x) = \langle H_0(x) \rangle + H_0'(x) \tag{2c}$$

where < > stands for ensemble average and ' for perturbation. The initial condition $H_0(x)$ in (1) can be any function. For the conceptualization of the groundwater flow presented in Fig. 1, the steady-state condition can be reached in this aquifer after a rainfall or during a wet season. Thus the steady-state solution to this model were often adopted as initial condition in previous research (Liang and Zhang, 2012, 2013a, b). Thus, in this study, we set initial condition $H_0(x)$ to be the steady-state solution to the one-dimensional groundwater flow equation, i.e., $H_0(x) = h_0 + 0.5W_0(L^2 - x^2)/T$, where h_0 [L] is the constant groundwater level at the right boundary and W_0 [L/T] is the spatially constant recharge rate (Liang and Zhang, 2012). Since h_0 is taken to be constant, the source of the uncertainty in the initial head $H_0(x)$ is due to random W_0 only. Thus, the mean and perturbation of $H_0(x)$ can be written as, $\langle H_0(x) \rangle = h_0 + 0.5\langle W_0 \rangle (L^2 - x^2)/T$ and $H_0'(x) = 0.5W_0'(L^2 - x^2)/T$, respectively. By substituting Eq. (2), $\langle H_0(x) \rangle$, and $H_0'(x)$ into Eq. (1) and taking expectation, one obtains the mean flow equation with the mean initial and boundary conditions as

$$T\frac{\partial^2 \langle h \rangle}{\partial x^2} + \langle W \rangle = S_Y \frac{\partial \langle h \rangle}{\partial t} \tag{3a}$$

130 $$\langle h(x,0)\rangle = h_0 + \frac{\langle W_0\rangle}{2T}\left(L^2 - x^2\right);\;\; T\frac{\partial\langle h\rangle}{\partial x}\Big|_{x=0} = \langle Q\rangle;\;\; \langle h(L,t)\rangle = \langle H(t)\rangle \tag{3b}$$

131 Subtracting Eq. (3) from (1) leads to the following perturbation equation with the
132 initial and boundary conditions

133 $$T\frac{\partial^2 h'}{\partial x^2} + W' = S_Y\frac{\partial h'}{\partial t} \tag{4a}$$

134 $$h'(x,0) = \frac{W_0'}{2T}\left(L^2 - x^2\right);\quad T\frac{\partial h'}{\partial x}\Big|_{x=0} = Q';\;\; h'(L,t) = H'(t) \tag{4b}$$

135 The analytical solution to Eq. (4) can be derived with integral-transform methods
136 (Ozisik, 1968) given by

137 $$h' = \frac{2}{L}\sum_{n=0}^{\infty} e^{-\beta b_n^2 t}\cos(b_n x)\left[\frac{(-1)^n}{b_n^3 T}W_0' + \beta\int_0^t e^{\beta b_n^2\xi}\left[\frac{(-1)^n}{Tb_n}W'(\xi) - \frac{Q'(\xi)}{T} + H'(\xi)(-1)^n b_n\right]d\xi\right] \tag{5}$$

138 where $\beta = T/S_Y$, $b_n = (2n+1)\pi/(2L)$. Using Eq. (5), the temporal covariance of the
139 groundwater level fluctuations can be derived as

140 $$\begin{aligned} &C_{hh}(x,t_1;x,t_2) = E[h'(x,t_1)h'(x,t_2)] \\ &= \frac{4}{L^2}\sum_{m=0}^{\infty}\sum_{n=0}^{\infty} e^{-\beta\left(b_m^2 t_1 + b_n^2 t_2\right)}\cos(b_m x)\cos(b_n x)\left[\frac{(-1)^{m+n}}{T^2 b_m^3 b_n^3}\sigma_{W_0}^2\right. \\ &\left. + \beta^2\int_0^{t_1}\int_0^{t_2} e^{\beta\left(b_m^2\xi + b_n^2\rho\right)}\left[\frac{(-1)^{n+m}}{T^2 b_m b_n}C_{WW}(\xi,\rho) + \frac{C_{QQ}(\xi,\rho)}{T^2} + C_{HH}(\xi,\rho)(-1)^{m+n}b_m b_n\right]d\xi d\rho\right] \end{aligned} \tag{6}$$

141 in which $\sigma_{W_0}^2$ is the variance of W_0, and $C_{WW}(\xi,\rho), C_{QQ}(\xi,\rho)$ and $C_{HH}(\xi,\rho)$ are the
142 temporal auto-covariance of *W(t)*, of *Q(t)*, and *H(t)*, respectively. We assume that
143 *W(t)*, Q*(t)*, and *H(t)* are uncorrelated in order to simplify our analyses. It is shown in
144 Eq. (6) that the head covariance depends on the variance of W_0 and the covariances
145 of *W(t)*, Q*(t)*, and *H(t)* and this equation can be evaluated for any random *W(t)*, Q*(t)*,
146 and *H(t)*. We assume that these processes are white noises as employed in previous

studies (Gelhar, 1993;Hantush and Marino, 1994;Liang and Zhang, 2013a). More realistic randomness of these processes will be considered in future studies.

Following *Gelhar* (1993, p.34), we express the spectra of *W(t)*, Q*(t)*, and *H(t)* as $S_{WW}=\sigma_W^2\lambda_W/\pi$, $S_{QQ}=\sigma_Q^2\lambda_Q/\pi$, and $S_{HH}=\sigma_H^2\lambda_H/\pi$, respectively, where σ_W^2, σ_Q^2, and σ_H^2 are the variances and λ_W, λ_Q, and λ_H are the correlation time intervals of these three processes, respectively. The corresponding covariance of *W(t), Q(t)* and *H(t)* are $C_{WW}(\xi,\rho)=2\sigma_W^2\lambda_W\delta(\xi-\rho)$, $C_{QQ}(\xi,\rho)=2\sigma_Q^2\lambda_Q\delta(\xi-\rho)$, and $C_{HH}(\xi,\rho)=2\sigma_H^2\lambda_H\delta(\xi-\rho)$. Substituting these covariance into (6) and taking integration, one obtain analytical solution of head covariance

$$C_{hh}(x',t',\tau')=\frac{4\beta L^2}{T^2}\sum_{m=0}^{\infty}\sum_{n=0}^{\infty}\cos(b'_m x')\cos(b'_n x')\left\{e^{-\left[\left(b'^2_m+b'^2_n\right)t'+\left(b'^2_n-b'^2_m\right)\frac{\tau'}{2}\right]}\frac{L^2(-1)^{m+n}\sigma^2_{W_0}}{\beta b'^3_m b'^3_n}\right.$$
$$\left.+2\frac{\left(e^{-b'^2_m\tau'}-e^{-2b'^2_m t'}\right)}{\left(b'^2_m+b'^2_n\right)}\left[\frac{(-1)^{m+n}\sigma_W^2\lambda_W}{b'_m b'_n}+\frac{\sigma_Q^2\lambda_Q}{L^2}+\frac{(-1)^{m+n}b'_m b'_n T^2\sigma_H^2\lambda_H}{L^4}\right]\right\} \quad (7)$$

where $\tau'=t'_2-t'_1$ and $t'=(t'_2+t'_1)/2$. The analytical solution for the head variance can be obtain by setting $\tau'=0$

$$\sigma_h^2(x',t')=\frac{4\beta L^2}{T^2}\sum_{m=0}^{\infty}\sum_{n=0}^{\infty}\cos(b'_m x')\cos(b'_n x')\left\{e^{-\left(b'^2_m+b'^2_n\right)t'}\frac{L^2}{\beta}\frac{(-1)^{m+n}\sigma^2_{W_0}}{b'^3_m b'^3_n}+\right.$$
$$\left.2\frac{1-e^{-2b'^2_m t'}}{\left(b'^2_m+b'^2_n\right)}\left[\frac{(-1)^{m+n}\sigma_W^2\lambda_W}{b'_m b'_n}+\frac{\sigma_Q^2\lambda_Q}{L^2}+\frac{(-1)^{m+n}b'_m b'_n T^2\sigma_H^2\lambda_H}{L^4}\right]\right\} \quad (8)$$

where

$$t'=\frac{t}{t_c};\quad x'=\frac{x}{L};\quad t_c=\frac{L^2}{\beta};\quad b'_n=\frac{(2n+1)\pi}{2}$$

in which $t_c(=S_Y L^2/(KM))$ [1/T] is a characteristic timescale (Gelhar, 1993) where the transmissivity (*T*) is replaced by the product of the hydraulic conductivity (*K*) and the average saturated thickness (*M*) of the aquifer. The characteristic timescale (t_c) is

an important parameter and its value for most shallow aquifers is usually larger than 100 day since the horizontal extent of a shallow aquifer is usually much larger than its thickness. For instance, the value of t_c is 250 days for a sandy aquifer with L=100m, M =10m, K=1m/day, and S_Y=0.25.

The spectral density of *h(x, t)* can't be derived by ordinary Fourier transform since the head covariance and variance depend on time *t'* and thus *h(x, t)* are temporally non-stationary as shown in Eqs. (7) and (8). Priestley (1981) defined the spectral density of non-stationary processes (Wigner spectrum) as the Fourier transform of time-dependent auto-covariance with fixed reference time *t* and derived time-dependent spectral density. In order to obtain the spectrum of *h(x, t)*, we applied Priestley's method and obtained the time-dependent spectral density (Priestley, 1981; Zhang and Li, 2005;Liang and Zhang, 2013a), i.e.,

$$
\begin{aligned}
&S_{hh}(x,t,\omega)=\frac{1}{2\pi}\int_{-\infty}^{\infty}C_{hh}(x,t,\tau)e^{-i\omega\tau}d\tau \\
&=\sum_{m=0}^{\infty}\sum_{n=0}^{\infty}\cos(b_m x)\cos(b_n x)\frac{2t_c\left(b_n^2-b_m^2\right)e^{-\beta\left(b_m^2+b_n^2\right)t}}{\beta^2\left(b_n^2-b_m^2\right)^2/4+\omega^2}\frac{(-1)^{m+n}\sigma_{W_0}^2}{\pi T^2 b_m^3 b_n^3}+ \\
&\sum_{m=0}^{\infty}\sum_{n=0}^{\infty}\cos(b_m x)\cos(b_n x)\frac{8\beta b_m^2}{t_c\left(b_m^2+b_n^2\right)}\frac{1}{\beta^2 b_m^4+\omega^2}\left[\frac{(-1)^{m+n}S_{WW}}{T^2 b_m b_n}+\frac{S_{QQ}}{T^2}+(-1)^{m+n}b_m b_n S_{HH}\right]
\end{aligned}
\tag{9}
$$

where ω is angular frequency and $\omega = 2\pi f$, f is frequency, and $i=\sqrt{-1}$. It is seen in Eq. (9) that the spectrum S_{hh} is dependent on not only frequency and locations but also time *t*. The time-dependent term (i.e., first term) in Eq. (9) is caused by the random initial condition and is proportional to $e^{-\beta\left(b_m^2+b_n^2\right)t}$ which decays quickly with *t*. We evaluated the first term in the Eq. (9) by setting *t*=0 and found that it is much smaller than the second term in Eq. (9). We thus ignored the first term and evaluated the spectrum using the approximation,

$$S_{hh}(x',\omega)=\sum_{m=0}^{\infty}\sum_{n=0}^{\infty}\frac{8\beta b'^{2}_{m}\cos(b'_{m}x')\cos(b'_{n}x')}{t_c\left(b'^{2}_{m}+b'^{2}_{n}\right)\left(\beta^{2}b'^{4}_{m}/L^{4}+\omega^{2}\right)}\left[\frac{(-1)^{m+n}S_{WW}L^{2}}{T^{2}b'_{m}b'_{n}}+\frac{S_{QQ}}{T^{2}}+\frac{(-1)^{m+n}b'_{m}b'_{n}S_{HH}}{L^{2}}\right] \quad (10)$$

3. Results and Discussion

3.1 Variance of groundwater levels

The general expression of the head variance in Eq. (8) depends on the variances of the four random processes, $\sigma^2_{W_0}$, σ^2_W, σ^2_Q, and σ^2_H. In the following we will study their individual and combined effects on the head variation and focus our attention only on the variance of *h(x, t)*. The dimensionless standard deviation of *h(x, t)*, σ'_h, or the square root of the dimensionless variance (σ'^2_h) as a function of the dimensionless time (*t'*) were evaluated and presented in the left column of Fig. 2 at fixed dimensionless locations (*x'*). The σ'_h as a function of *x'* was evaluated and presented in the right column of Fig. 2 at fixed *t'*.

We first evaluate the effect of the random initial condition due to the random term, W_0, by setting $\sigma^2_W=\sigma^2_Q=\sigma^2_H=0$. In this case the dimensionless variance in Eq. (8) reduces to

$$\sigma'^2_h(x',t')=\sum_{m=0}^{\infty}\sum_{n=0}^{\infty}\frac{(-1)^{m+n}}{b'^3_m b'^3_n}\cos(b'_m x')\cos(b'_n x')e^{-\left(b'^2_m+b'^2_n\right)t'} \quad (11)$$

where $\sigma'^2_h=\sigma^2_h T^2/(4L^4\sigma^2_{W_0})$. The changes of the σ'_h with *x'* and *t'* were presented in Fig 2a and 2b, respectively. It is shown in Fig. 2a that for a fixed location the σ'_h is at its maximum at *t'*=0 and decreases with time gradually to a negligible number at *t'*=1.0. This means that the error in *h(x, t)* predicted by an analytical or numerical solution due to the uncertain initial condition is significant at

206 early time, especially near a flux boundary. The time duration during which the
207 effect of the uncertain initial condition is significant depends on the value of the
208 characteristic timescale (t_c) since $t'=t/t_c$. In the most aquifers this duration may last
209 many days. In the typical aquifer studied the effect of the uncertainty in initial
210 condition on *h(x, t)* is significant during first 250 days (t'=1.0). This duration should
211 be relatively short, however, in a more permeable aquifer whose horizontal extent (L)
212 is relatively smaller than its thickness (M). It is seen in Fig. 2b that for a fixed time，
213 the σ'_h is the largest at the left flux boundary (x'=0.0) and becomes zero at the right
214 constant head boundary (x'=1.0) since the right boundary is deterministic. This
215 means that the error in *h(x, t)* predicted by an analytical or numerical solution due to
216 the uncertain initial condition is significant almost everywhere in the aquifer: the
217 further away from a constant head boundary, the larger the error.

218 We then consider the uncertainty in the areal source/sink term (W) by setting
219 $\sigma^2_{W_0} = \sigma^2_Q = \sigma^2_H = 0$. In this case the dimensionless variance in Eq. (8) reduces to

220 $$\sigma'^2_h(x',t') = 2\sum_{m=0}^{\infty}\sum_{n=0}^{\infty}\cos(b'_m x')\cos(b'_n x')\frac{(1-e^{-2b'^2_m t'})(-1)^{m+n}}{(b'^2_m+b'^2_n)b'_m b'_n} \qquad (12)$$

221 where $\sigma'^2_h = \sigma^2_h TS_Y/(4L^2\sigma^2_W\lambda_W)$. The changes of the σ'_h with x' and t' were
222 presented in Fig 2c and 2d, respectively. It is noticed in Fig. 2c that at a fixed location,
223 the σ'_h is zero initially, gradually increases as time goes, and approaches a constant
224 limit at later time. This means that the error in *h(x, t)* due to an source/sink is at its
225 minimum at early time and increases with time to approach a constant limit at later
226 time: the closer to the left flux boundary, the larger the limit. For a fixed time the
227 σ'_h decreases smoothly from the left to the right boundary (Fig. 2d). The error in *h(x,*

t) due to the uncertainty in the source/sink is significant almost everywhere in the aquifer: the further away from the constant head boundary, the larger the error, similar to the previous case with the random initial condition (Fig. 2b).

Thirdly, we investigate the effect of the left random flux boundary by setting $\sigma_{W_0}^2 = \sigma_W^2 = \sigma_H^2 = 0$ in Eq. (8). In this case the dimensionless head variance is given by

$$\sigma'^2_h(x',t') = 2\sum_{m=0}^{\infty}\sum_{n=0}^{\infty}\cos(b'_m x')\cos(b'_n x')\frac{1-e^{-2b'^2_m t'}}{b'^2_m + b'^2_n} \qquad (13)$$

where $\sigma'^2_h = \sigma_h^2 TS_Y/(4\sigma_Q^2\lambda_Q)$. The changes of the σ'_h with *x'* and *t'* were presented in Fig 2e and 2f, respectively. At any location the σ'_h in Fig. 2e or the error in *h(x, t)* due to an uncertain flux boundary is at its minimum at early time and increases quickly with time to approach a constant limit: the closer to the left flux boundary, the larger the limit. At any time the σ'_h in Fig. 2f or the error in the head due to the uncertain flux boundary is at its maximum at the left boundary but decreases quickly away from the boundary to become insignificant for *x'*>0.8.

Fourthly, we investigated the effect of the random head boundary by setting $\sigma_{W_0}^2 = \sigma_W^2 = \sigma_Q^2 = 0$ in Eq. (8). The dimensionless head variance in this case is given by

$$\sigma'^2_h(x',t') = 2\sum_{m=0}^{\infty}\sum_{n=0}^{\infty}\cos(b'_m x')\cos(b'_n x')\frac{(-1)^{m+n} b'_m b'_n\left(1-e^{-2b'^2_m t'}\right)}{\left(b'^2_m + b'^2_n\right)} \qquad (14)$$

where $\sigma'^2_h = \sigma_h^2 L^2 S_Y/(4T\sigma_H^2\lambda_H)$. The changes of this σ'_h with *x'* and *t'* were presented in Fig 2g and 2h, respectively. It seen in Fig. 2g that at any location the σ'_h or the error in *h(x, t)* due to the random head boundary increases with time

quickly to approach a constant limit: the closer to the uncertain head boundary, the larger the error. The spatial variation of σ'_h can be clearly observed in Fig. 2h for fixed *t'*. At any time σ'_h is at its maximum at the right boundary (*x'*=1) where the head is uncertain, decreases quickly away from the boundary. The error in *h(x, t)* due to the uncertain head boundary is limited in a narrow zone near the boundary (*x'*>0.8) (Fig. 2h).

Finally, we consider the combined effects of the uncertainties from all four sources, i.e., the initial condition, sources, and flux and head boundaries. The head variance in Eq. (8) is written in the dimensionless form as

$$\sigma'^2_h(x',t') = \sum_{m=0}^{\infty}\sum_{n=0}^{\infty}\cos(b'_m x')\cos(b'_n x')\left\{e^{-(b'^2_m+b'^2_n)t'}\frac{(-1)^{m+n}\sigma'^2_{W_0}}{b'^3_m b'^3_n} + 2\frac{1-e^{-2b'^2_m t'}}{(b'^2_m+b'^2_n)}\left[\frac{(-1)^{m+n}}{b'_m b'_n}+\sigma'^2_Q+(-1)^{m+n}b'_m b'_n \sigma'^2_H\right]\right\} \quad (15)$$

where

$$\sigma'^2_h = \frac{\sigma_h^2 T S_Y}{4L^2\sigma_W^2\lambda_W};\ \sigma'^2_{W_0} = \frac{L^2 S_Y \sigma^2_{W_0}}{T\sigma_W^2\lambda_W};\ \sigma'^2_Q = \frac{\sigma_Q^2\lambda_Q}{L^2\sigma_W^2\lambda_W};\ \sigma'^2_H = \frac{T^2\sigma_H^2\lambda_H}{L^4\sigma_W^2\lambda_W}$$

The dimensionless variances, $\sigma'^2_{W_0}$, σ'^2_Q and σ'^2_H, need to be specified in order to evaluate the dimensionless $\sigma'^2_h(x',t')$ in Eq. (15). For the typical aquifer mentioned above with *L*=100m, *T*=10 m^2/day (or *K*=1m/day and *M*=10m) and S_Y=0.25, we set $\sigma^2_{W_0}/(\sigma_W^2\lambda_W)=10^{-1}$, $\sigma_Q^2\lambda_Q/(\sigma_W^2\lambda_W)=10^3$, $\sigma_H^2\lambda_H/(\sigma_W^2\lambda_W)=10^4$ and obtain $\sigma'^2_{W_0}=25$, $\sigma'^2_Q=0.1$ and $\sigma'^2_H=0.01$.

The changes of this σ'_h with *x'* and *t'* were presented in Fig 2i and 2j, respectively. It is observed in Fig. 2i that at any location the σ'_h is at its maximum

due to the uncertainty in the initial condition, gradually decreases as time goes, and approaches a constant limit at later time (t'>0.6) which is due to the combined effects of the uncertain source/sink and flux and head boundaries. This means that the error in the head in early time is significant if the initial condition is uncertain and reduces as time goes to reach a constant limit. The error in head in later time is determined by the uncertainties in the source/sink, flux and head boundaries. It can be observed in Fig. 2j that σ'_h is relatively larger near both boundaries. The values of σ'_h at the two boundaries are equivalent (~1.3) at early time, say t'=0.01 (the top curve in Fig. 2j) and it reduces slowly away from the flux boundary but quickly away from the head boundary. As time progresses, the σ'_h near the head boundary stays more or less the same but reduces significantly in most part of the aquifer. This means that in early time the error in *h(x, t)* in most part of the aquifer is mainly caused by the initial condition and at later time it is due to the combined effects of the uncertain areal source/sink and flux boundary. The effect of the uncertain head boundary on *h(x, t)* doesn't change with time significantly but is limited in a narrow zone near the boundary.

3.2 Spectrum of groundwater levels

We first evaluated S_{hh} in Eq. (10) due to the effect of the white noise flux boundary only by setting $S_{QQ} \neq 0$, $S_{WW} = 0$, and $S_{HH} = 0$. The dimensionless spectrum S_{hh}/S_{QQ} as a function of the frequency (f) was evaluated and presented in the log-log plot (Fig. 3a-3c) for three values of t_c (40, 400, and 4,000 days) since the value of t_c is 250 days for a sandy aquifer as we mentioned above and at the six

290 locations (*x'* = 0.0, 0.2, 0.4, 0.6, 0.8, and 0.9). The spectrum S_{hh}/S_{QQ} in Fig. 3a is
291 more or less horizontal (i.e., white noise) at low frequencies and decrease gradually
292 as *f* increases, indicating that an aquifer acts as a low-bass filter that filter signals at
293 high frequencies and keep signals at low frequencies. The aquifer has significantly
294 dampened the fluctuations of the groundwater level. The spectrum varies with the
295 location *x'*: the smaller the value of *x'* or the closer to the left flux boundary (*x'*=0),
296 the larger the spectrum (Fig. 3a-3c). All spectra in Fig. 3a are not a straight line in
297 the log-log plot, meaning that the temporal scaling of *h(x, t)* doesn't exist in the
298 range of f =10^{-3}~10^{0} when t_c=40 days. As t_c increases to 400 and 4000 days,
299 however, the spectrum at *x'*=0 become a straight line (the top curve in Fig. 3b and 3c)
300 or has a power-law relation with *f*, i.e., $S_{hh}/S_{QQ} \propto 1/f$, since its slope is approximately
301 one. The fluctuations of *h(0, t)* is a pink noise due to the white noise fluctuations flux
302 boundary when the characteristic timescale (t_c) is large which means that the aquifer
303 is relatively less permeable and/or has a much larger horizontal length than its
304 thickness.

305 Secondly, the spectrum S_{hh}/S_{HH} due to the sole effect of the random head
306 boundary was evaluated by setting $S_{HH} \neq 0$, $S_{WW} = 0$, and $S_{QQ} = 0$ in Eq. (10) for
307 the same three values of t_c and six locations and presented in Fig. 3d-3f as a function
308 of *f*. It is shown that similar to Fig. 3a-3c, the spectrum decreases as *f* increases but
309 different from Fig. 3a-3c, the spectrum is larger at *x'*=0.9 near the right boundary
310 (the top curves in Fig. 3d-3f) than that *x'*=0.0 (the bottom curves). Furthermore,
311 none of the spectra are a straight line in the log-log plot, indicating that the temporal

312 scaling of groundwater level fluctuations doesn't exist in the case of the white noise
313 head boundary.

314 Thirdly, the spectrum S_{hh}/S_{WW} due the effect of the white noise recharge only
315 was evaluated by setting $S_{WW} \neq 0$, $S_{QQ} = 0$, and $S_{HH} = 0$ in Eq. (10) for the same
316 values of t_c and x' and presented in Fig. 3g-3i as a function of f. It is shown that
317 when t_c=40 day the spectrum in Fig. 3g is horizontal at low frequencies and become
318 a straight line at high frequencies: the closer to the right head boundary, the later it
319 approaches a straight line (Fig. 3h). As t_c increases to 400 and 4000 days, the slope
320 of the spectrum at all locations except at x'=0.9 approaches to a straight line with a
321 slope of 2 (Fig. 3h and 3i), indicating a temporal scaling of $h(x, t)$. The fluctuations
322 of groundwater level is a Brownian motion, i.e., $S \propto 1/f^2$, when $t_c \geq 4000$ day or in
323 a relatively less permeable and/or has a much larger horizontal length than its
324 thickness.

325 Finally, the head spectrum due to the combined effect of all three random
326 sources (the white noise recharge, and flux and head boundaries) was evaluated, i.e.,
327 $S_{WW} \neq 0$, $S_{QQ} \neq 0$, and $S_{HH} \neq 0$ in Eq. (10). The spectrum of S_{hh}/S_{WW} as a
328 function of f was presented in Fig. 3j-3l for the same values of t_c and x' where
329 $S_{QQ}/S_{WW} = 1000$ and $S_{HH}/S_{WW} = 10000$ which are same with the values using in
330 previous section. It is noticed that the general patterns of S_{hh}/S_{WW} in the
331 combined case is similar to the case under the random source/sink only (Fig. 3g-3i)
332 except at x'=0.0 and 0.9 (the dashed and dotted curves in Fig. 3j, respectively) due
333 to the strong effects of the boundary conditions at these two locations. At t_c=4000

day, the spectra at all locations except x'=0.0 (Fig. 3l) are similar to those in Fig. 3i, indicating the dominating effect of the random areal source/sink. The spectrum at x'=0 in this case is also a straight line (the dashed curve in Fig. 3l) but with a different slope due to the effect of the random flux boundary which is similar to the top straight line in Fig. 3c. Above results provide a theoretical explanation as why temporal scaling exists in the observed groundwater level fluctuations (Zhang and Schilling, 2004;Bloomfield and Little, 2010;Zhu et al., 2012). We thus conclude that temporal scaling of $h(x, t)$ may indeed exist in real aquifers due to the strong effect of the areal source/sink.

4. Conclusions

In this study the effects of random source/sink, and initial and boundary conditions on the uncertainty and temporal scaling of the groundwater level, $h(x, t)$ were investigated. The analytical solutions for the variance, covariance and spectrum of $h(x, t)$ in an unconfined aquifer described by a linearized Boussinesq equation with white noise source/sink, and initial and boundary conditions were derived. The standard deviations of $h(x, t)$ for various cases were evaluated. Based on the results, the following conclusions can be drawn.

1. The error in $h(x, t)$ due to a random initial condition is significant at early time, especially near a flux boundary. The duration during which the effect is significant may last a few hundred days in most aquifers;

2. The error in $h(x, t)$ due to a random areal source/sink is significant in most part of an aquifer: the closer to a flux boundary, the larger the error;

3. The errors in $h(x, t)$ due to random flux and head boundaries are significant near the boundaries: the closer to the boundaries, the larger the errors. The random flux boundary may affect the head over a larger region near the boundary than the random head boundary;

4. In the typical sandy aquifer studied (with the length of aquifer at the direction of water flow L=100m, the average saturated thickness M =10m, hydraulic conductivity K=1m/day, and specific yield S_Y=0.25) the error in $h(x, t)$ in early time is mainly caused by an uncertain initial condition and the error reduces as time goes to reach a constant error in later time. The constant error in $h(x, t)$ is mainly due to the combined effects of uncertain source/sink and boundaries;

5. The aquifer system behaves as a low-pass filter which filter the short-term (high frequencies) fluctuations and keep the long-term (low frequencies) fluctuations;

6. Temporal scaling of groundwater level fluctuations may indeed exist in most part of a low permeable aquifer whose horizontal length is much larger than its thickness caused by the temporal fluctuations of areal source/sink.

Finally, it is pointed out that the analyses carried out in this study is under the assumptions that the processes, $W(t)$, $Q(t)$, and $H(t)$ are uncorrelated white noises. In reality, they may be correlated and spatially varied. We plan to relax those constrains and study more realistic cases in the near future. It is also noted that the analytical solutions for head variances derived in this study provide a way to identify and quantify the uncertainty. The spectrum relationship obtained among the head,

recharge and boundary conditions can help one to improve spectrum analysis for a groundwater level time series and removed the effects of the boundary conditions.

Acknowledgment

This study was partially supported with the research grants from the National Nature Science Foundation of China (NSFC-41272260; NSFC-41330314; NSFC-41302180), the Natural Science Foundation of Jiangsu Province (SBK201341336) and from the National Key project "Water Pollution Control in the Huai River Basin" of China (2012ZX07204-001, 2012ZX07204-003).

References

Bear, J.: Dynamics of fluids in porous media, Environmental science series (New York, 1972-), American Elsevier Pub. Co., New York,, xvii, 764 p. pp., 1972.

Beven, K., and Binley, A.: The Future of Distributed Models - Model Calibration and Uncertainty Prediction, Hydrol Process, 6, 279-298, 1992.

Bloomfield, J. P., and Little, M. A.: Robust evidence for random fractal scaling of groundwater levels in unconfined aquifers, J Hydrol, 393, 362-369, DOI 10.1016/j.jhydrol.2010.08.031, 2010.

Dagan, G.: Flow and transport in porous formations, Springer-Verlag, Berlin ; New York, xvii, 465 p. pp., 1989.

Gelhar, L. W.: Stochastic subsurface hydrology, Prentice-Hall, Englewood Cliffs, N.J., x, 390 p. pp., 1993.

Hantush, M. M., and Marino, M. A.: One-Dimensional Stochastic-Analysis in Leaky Aquifers Subject to Random Leakage, Water Resour Res, 30, 549-558, Doi 10.1029/93wr02887, 1994.

Liang, X. Y., and Zhang, Y. K.: A new analytical method for groundwater recharge and discharge estimation, J Hydrol, 450, 17-24, DOI 10.1016/j.jhydrol.2012.05.036, 2012.

Liang, X. Y., and Zhang, Y. K.: Temporal and spatial variation and scaling of groundwater levels in a bounded unconfined aquifer, J Hydrol, 479, 139-145, DOI 10.1016/j.jhydrol.2012.11.044, 2013a.

Liang, X. Y., and Zhang, Y. K.: Analytic solutions to transient groundwater flow under time-dependent sources in a heterogeneous aquifer bounded by fluctuating river stage, Adv Water Resour, 58, 1-9, DOI 10.1016/j.advwatres.2013.03.010, 2013b.

Neuman, S. P.: Maximum likelihood Bayesian averaging of uncertain model predictions, Stoch Env Res Risk A, 17, 291-305, 10.1007/s00477-003-0151-7, 2003.

Neuman, S. P., Xue, L., Ye, M., and Lu, D.: Bayesian analysis of data-worth considering model and parameter uncertainties, Advances in Water Resources, 36, 75-85, 10.1016/j.advwatres.2011.02.007, 2012.

412 Nowak, W., de Barros, F. P. J., and Rubin, Y.: Bayesian geostatistical design: Task-driven optimal site
413 investigation when the geostatistical model is uncertain, Water Resour Res, 46, Artn W03535
414 Doi 10.1029/2009wr008312, 2010.
415 Priestley, M. B.: Spectral Analysis and Time Series, Academic Press, San Diego, 1981.
416 Refsgaard, J. C., van der Sluijs, J. P., Hojberg, A. L., and Vanrolleghem, P. A.: Uncertainty in the
417 environmental modelling process - A framework and guidance, Environmental Modelling &
418 Software, 22, 1543-1556, 10.1016/j.envost.2007.02.004, 2007.
419 Rojas, R., Feyen, L., and Dassargues, A.: Conceptual model uncertainty in groundwater modeling:
420 Combining generalized likelihood uncertainty estimation and Bayesian model averaging, Water
421 Resources Research, 44, 10.1029/2008wr006908, 2008.
422 Rojas, R., Feyen, L., Batelaan, O., and Dassargues, A.: On the value of conditioning data to reduce
423 conceptual model uncertainty in groundwater modeling, Water Resources Research, 46, 20,
424 10.1029/2009wr008822, 2010.
425 Schilling, K. E., and Zhang, Y. K.: Temporal Scaling of Groundwater Level Fluctuations Near a
426 Stream, Ground Water, 50, 59-67, DOI 10.1111/j.1745-6584.2011.00804.x, 2012.
427 Vrugt, J. A., Gupta, H. V., Bouten, W., and Sorooshian, S.: A Shuffled Complex Evolution Metropolis
428 algorithm for optimization and uncertainty assessment of hydrologic model parameters, Water
429 Resources Research, 39, 10.1029/2002wr001642, 2003.
430 Ye, M., Meyer, P. D., and Neuman, S. P.: On model selection criteria in multimodel analysis, Water
431 Resources Research, 44, 10.1029/2008wr006803, 2008.
432 Zeng, X. K., Wang, D., Wu, J. C., and Chen, X.: Reliability Analysis of the Groundwater Conceptual
433 Model, Human and Ecological Risk Assessment, 19, 515-525, 10.1080/10807039.2012.713822,
434 2013.
435 Zhang, D.: Stochastic methods for flow in porous media : coping with uncertainties, Academic, San
436 Diego, Calif. London, xiv, 350 p. pp., 2002.
437 Zhang, Y. K., and Schilling, K.: Temporal scaling of hydraulic head and river base flow and its
438 implication for groundwater recharge, Water Resour Res, 40, -, Artn W03504
439 Doi 10.1029/2003wr002094, 2004.
440 Zhang, Y. K., and Li, Z. W.: Temporal scaling of hydraulic head fluctuations: Nonstationary spectral
441 analyses and numerical simulations, Water Resources Research, 41, 10.1029/2004wr003797,
442 2005.
443 Zhang, Y. K., and Li, Z. W.: Effect of temporally correlated recharge on fluctuations of groundwater
444 levels, Water Resources Research, 42, 10.1029/2005wr004828, 2006.
445 Zhang, Y. K., and Yang, X. Y.: Effects of variations of river stage and hydraulic conductivity on
446 temporal scaling of groundwater levels: numerical simulations, Stoch Env Res Risk A, 24,
447 1043-1052, DOI 10.1007/s00477-010-0437-5, 2010.
448 Zhu, J. T., Young, M. H., and Osterberg, J.: Impacts of riparian zone plant water use on temporal
449 scaling of groundwater systems, Hydrol Process, 26, 1352-1360, Doi 10.1002/Hyp.8241, 2012.
450
451

Figure captions

Figure 1 A schematic of the unconfined aquifer studied where $W(t)$ is the random time-dependent source/sink, $H_0(x)$ is the random initial condition, $Q(t)$ is the random time-dependent flux at the left boundary, $H(t)$ is the random time-dependent water level at the right boundary, L is distance from the left to the right boundary, and $h(x, t)$ is the random groundwater level in the aquifer.

Figure 2 The graphs on the left column are the standard deviation (σ'_h) of groundwater level ($h(x, t)$) versus the dimensionless time (t') at the dimensionless locations x'=0.0, 0.2, 0.4, 0.6, and 0.8. The graphs on the right column are σ'_h versus x' for the different t': b) and d) are for t'= 0.0, 0.2, 0.4, 0.6 and 0.8, f) and h) are for t'=0.01, 0.1, and 1.0, and j) is for t'=0.01, 0.2, 0.4, 0.6 and 0.8. Also, a) and b) are based on Eq.(11) where $\sigma_W^2 = \sigma_Q^2 = \sigma_H^2 = 0$; c) and d) are based on Eq. (12) where $\sigma_{W_0}^2 = \sigma_Q^2 = \sigma_H^2 = 0$; e) and f) are based on Eq. (13) where $\sigma_{W_0}^2 = \sigma_W^2 = \sigma_H^2 = 0$; g) and h) are based on Eq. (14) where $\sigma_{W_0}^2 = \sigma_W^2 = \sigma_Q^2 = 0$; i) and j) are based on Eq.(15) where $\sigma_{W_0}^2 \neq \sigma_W^2 \neq \sigma_Q^2 \neq \sigma_H^2 \neq 0$.

Figure 3 The dimensionless power spectrum versus frequency (f) at the dimensionless locations x'=0.0, 0.2, 0.4, 0.6, 0.8, and 0.9. The graphs on the left column are for t_c = 40 day, the graphs on the middle column are for t_c = 400 day, and the graphs on the right column are for t_c = 4000 day. The graphs on the first row are the dimensionless spectrum S_{hh}/S_{QQ} when $S_{WW} = 0$, $S_{HH} = 0$, and $S_{QQ} \neq 0$ in Eq. (10), the graphs on the second row is S_{hh}/S_{HH} when $S_{WW} = 0$, $S_{QQ} = 0$, and $S_{HH} \neq 0$, the graphs on the third row are S_{hh}/S_{WW} when $S_{QQ} = 0$, $S_{HH} = 0$, and $S_{WW} \neq 0$, and the graphs on the bottom row is S_{hh}/S_{WW} when $S_{QQ} \neq 0$, $S_{HH} \neq 0$, and $S_{WW} \neq 0$.

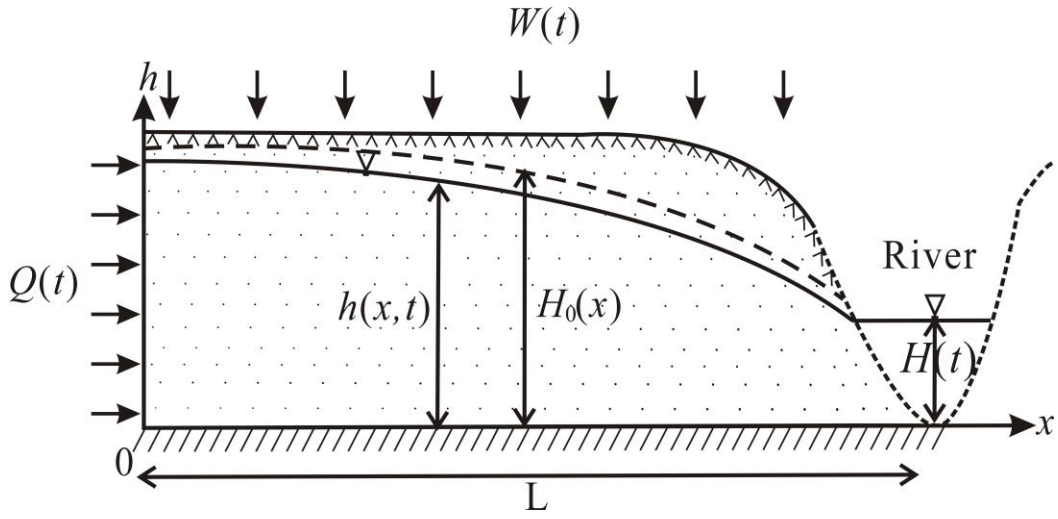

Figure 1

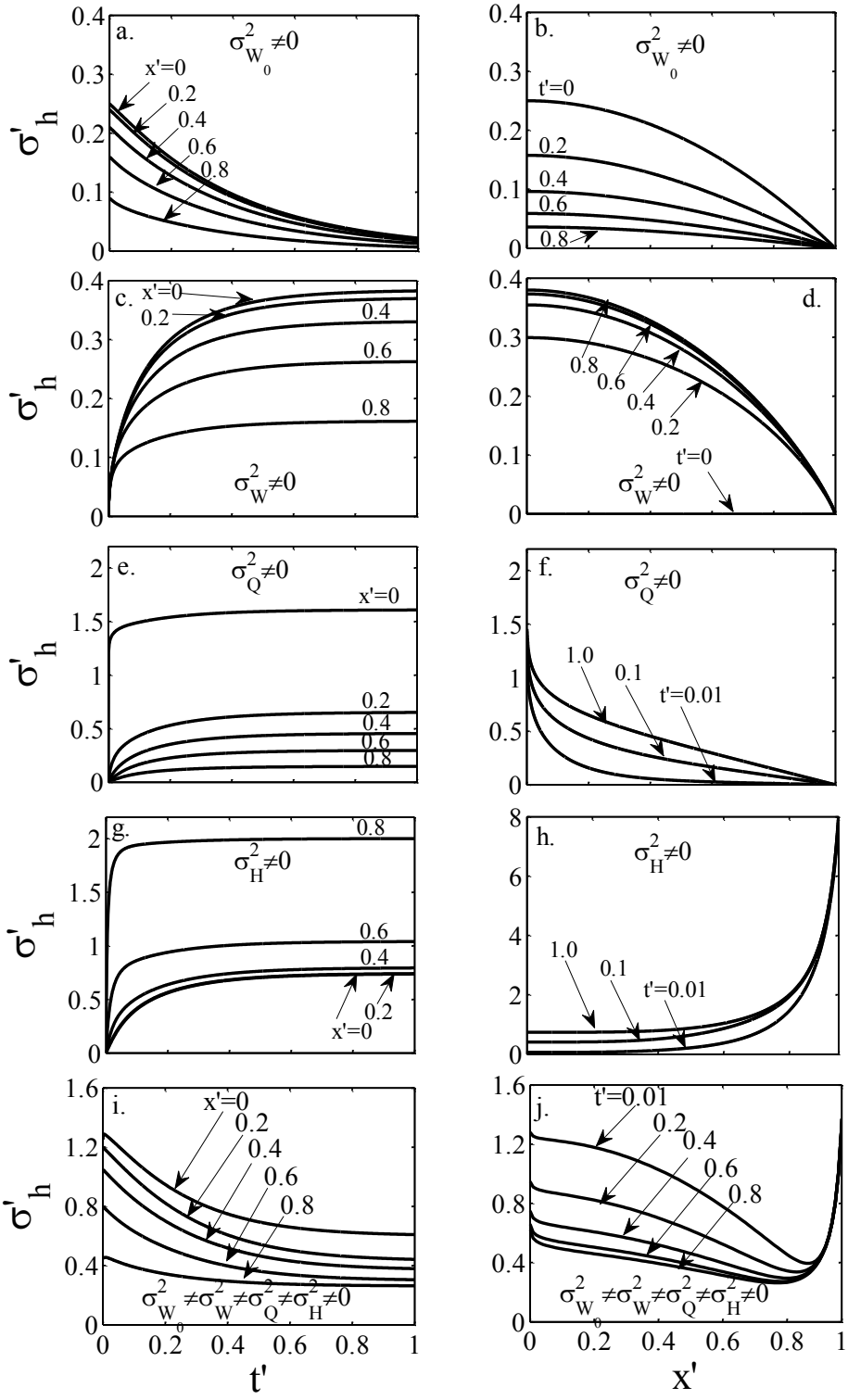
a.
$\sigma^2_{W_0} \neq 0$
x'=0
0.2
0.4
0.6
0.8
b.
$\sigma^2_{W_0} \neq 0$
t'=0
0.2
0.4
0.6
0.8
c.
x'=0
0.2
0.4
0.6
0.8
$\sigma^2_W \neq 0$
d.
0.8
0.6
0.4
0.2
t'=0
$\sigma^2_W \neq 0$
e.
$\sigma^2_Q \neq 0$
x'=0
0.2
0.4
0.6
0.8
f.
$\sigma^2_Q \neq 0$
1.0
0.1
t'=0.01
g.
0.8
$\sigma^2_H \neq 0$
0.6
0.4
0.2
x'=0
h.
$\sigma^2_H \neq 0$
1.0
0.1
t'=0.01
i.
x'=0
0.2
0.4
0.6
0.8
$\sigma^2_{W_0} \neq \sigma^2_W \neq \sigma^2_Q \neq \sigma^2_H \neq 0$
j.
t'=0.01
0.2
0.4
0.6
0.8
$\sigma^2_{W_0} \neq \sigma^2_W \neq \sigma^2_Q \neq \sigma^2_H \neq 0$
σ'_h
t'
x'

Figure 2

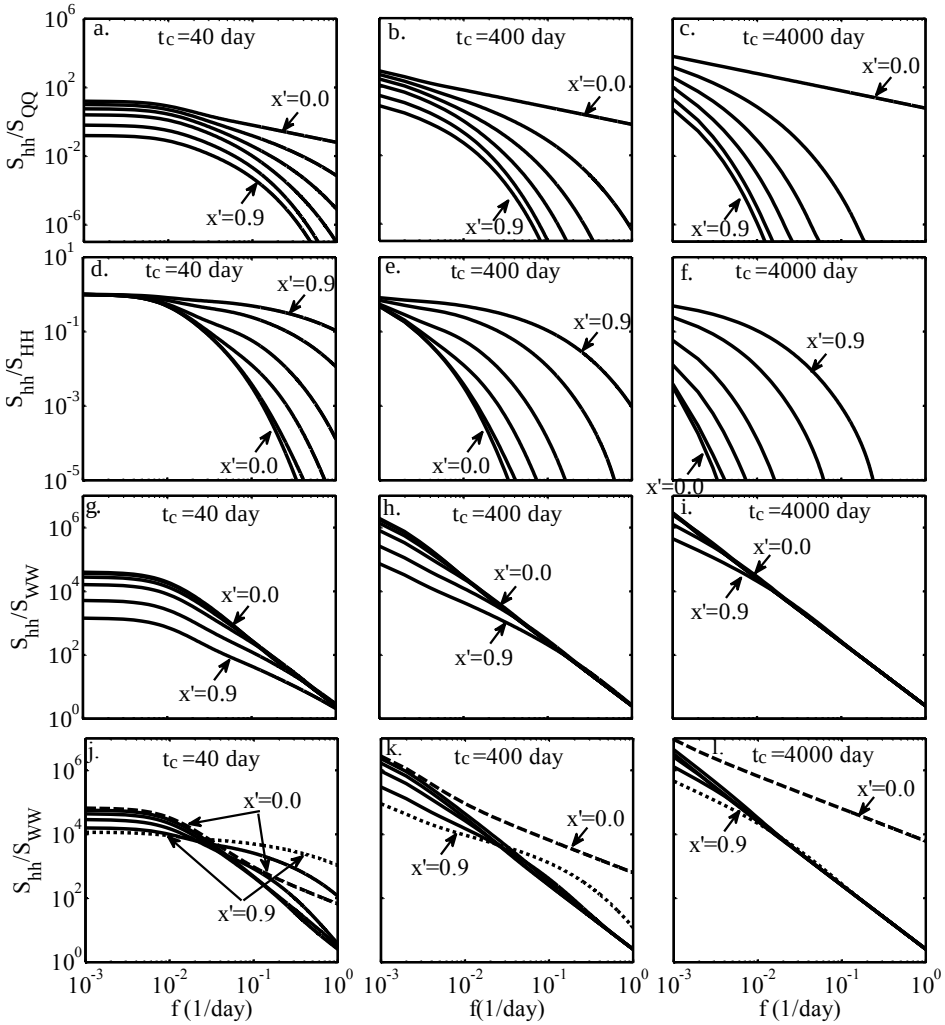
a.
tc =40 day
x'=0.0
x'=0.9
b.
tc =400 day
x'=0.0
x'=0.9
c.
tc =4000 day
x'=0.0
x'=0.9
d.
tc =40 day
x'=0.9
x'=0.0
e.
tc =400 day
x'=0.9
x'=0.0
f.
tc =4000 day
x'=0.9
x'=0.0
g.
tc =40 day
x'=0.0
x'=0.9
h.
tc =400 day
x'=0.0
x'=0.9
i.
tc =4000 day
x'=0.0
x'=0.9
j.
tc =40 day
x'=0.0
x'=0.9
k.
tc =400 day
x'=0.0
x'=0.9
l.
tc =4000 day
x'=0.0
x'=0.9
Shh/SQQ
Shh/SHH
Shh/SWW
Shh/SWW
f (1/day)
f(1/day)
f (1/day)

Figure 3

Technical note:

Analyses of Uncertainties and Scaling of Groundwater Level Fluctuations

Xiuyu Liang[a,b] , You-Kuan Zhang[a*,b,c]

[a]Center for Hydrosciences Research, Nanjing University,
Nanjing, Jiangsu 210093, P.R. China

[b]School of Earth Sciences and Engineering, Nanjing University,
Nanjing, Jiangsu 210093, P.R. China

[c]Department of Geoscience, University of Iowa,
Iowa City, Iowa 52242, USA

*Corresponding author
Phone: +86 25-83594485, Fax: +86 25-83596670,
Email: ykzhang@nju.edu.cn

~~Submitted~~ Resubmitted to *Hydrology and Earth System Sciences*
~~November~~May, ~~2014~~2015

带格式的：字体：加粗，倾斜
带格式的：字体：加粗，倾斜

Abstract

Analytical solutions for the variance, covariance, and spectrum of groundwater level, *h(x, t)*, in an unconfined aquifer described by a linearized Boussinesq equation with random source/sink and initial and boundary conditions were derived. It was found that in a typical aquifer the error in *h(x, t)* in early time is mainly caused by the random initial condition and the error reduces as time progresses to reach a constant error in later time. The duration during which the effect of the random initial condition is significant may last a few hundred days in most aquifers. The constant error in *h(x, t)* in later time is due to the combined effects of the uncertainties in the source/sink and flux boundary: the closer to the flux boundary, the larger the error. The error caused by the uncertain head boundary is limited in a narrow zone near the boundary and remains more or less constant over time. The aquifer system behaves as a low-pass filter which filters out high-frequency noises and keeps low-frequency variations. Temporal scaling of groundwater level fluctuations exists in most part of a low permeable aquifer whose horizontal length is much larger than its thickness caused by the temporal fluctuations of areal source/sink.

Key words: Uncertainty of groundwater levels; Temporal scaling; Random source/sink; Random initial and boundary conditions.~~Uncertainty and scaling of groundwater levels, Random source/sin and initial and boundary conditions.~~

1. Introduction

Groundwater level or hydraulic head (*h*) is the main driving force for water flow and advective contaminant transport in aquifers and thus the most important variable studied in groundwater hydrology and its applications. Knowledge about *h* is critical in dealing with groundwater-related environmental problems, such as over-pumping, subsidence, sea water intrusion, and contamination. One often found that the data about groundwater level is limited or unavailable in a hydrogeological investigation. In such cases the groundwater level distribution and its temporal variation are usually obtained with an analytical or numerical solution to a groundwater flow model.

It is obvious that errors always exit in the groundwater levels calculated or simulated with analytical or numerical solutions~~is obvious that there are some errors exit in Sspatiotemporal variations of groundwater levels calculated or simulated with the analytical or numerical solutions~~ in the realistic case~~ are inherently erroneous~~. The main sources of errors include the simplification or approximation in a conceptual model and the uncertainties in the model parameters. Problems in conceptualization or model structure were dealt with by many researchers (Neuman, 2003;Rojas et al., 2010;Ye et al., 2008;Rojas et al., 2008;Refsgaard et al., 2007;Zeng et al., 2013). The uncertainties in the model parameters (e.g., hydraulic conductivity, recharge rate, evapotranspiration, and river conductance) were investigated based on generalized likelihood uncertainty estimation and Bayesian methods ~~(Beven and Binley, 1992;Vrugt et al., 2003;Neuman et al., 2012)~~ (Nowak et al., 2010;Neuman et

带格式的：字体颜色：自动设置

带格式的：字体颜色：红色

带格式的：字体颜色：红色

带格式的：字体：小四

带格式的：字体：小四，非加粗，字体颜色：自动设置

al., 2012;Rojas et al., 2008;Rojas et al., 2010). The uncertainty in groundwater level has been one of the main research topics in stochastic subsurface hydrology for more than three decades. Most of these studies were focused on the spatial variability of groundwater level due to aquifers' heterogeneity (Dagan, 1989;Gelhar, 1993;Zhang, 2002). Little attention has been given to the uncertainties in groundwater level due to temporal variations of hydrological processes, e.g., recharge, evapotranspiration, discharge to a river, and river stage ~~(Bloomfield and Little, 2010;Zhang and Schilling, 2004;Schilling and Zhang, 2012;Liang and Zhang, 2013a;Zhu et al., 2012).~~ (Bloomfield and Little, 2010;Zhang and Schilling, 2004;Schilling and Zhang, 2012;Liang and Zhang, 2013a;Zhu et al., 2012).

Uncertainties of groundwater level fluctuations have been studied by Zhang and Li (2005, 2006) and most recently by Liang and Zhang (2013a). Based on a linear reservoir model with a white noise or temporally-correlated recharge process, Zhang and Li (2005, 2006) derived the variance and covariance of $h(t)$ by considering only a random source or sink process assuming deterministic initial and boundary conditions. Liang and Zhang (2013a) extended the studies of Zhang and Li (2005, 2006) and carried out non-stationary spectral analysis and Monte Carlo simulations using a linearized Boussinesq equation, and investigated the temporospatial variations of groundwater level. However, the only random process considered by Liang and Zhang (2013a) is the source/sink. Temporal scaling of groundwater levels discovered first by Zhang and Schilling Zhang and Schilling (2004) was verified in several studies (Zhang and Li, 2005, 2006; Bloomfield and Little, 2010; Zhang and

86 Yang, 2010; Zhu et al., 2012; Schilling and Zhang, 2012). However, we do not know
87 the effect of random boundary conditions on temporal scaling of groundwater levels.
88 In this study we extended above-mentioned work by considering the
89 groundwater flow in a bounded aquifer described by a linearized Boussinesq
90 equation with a random source/sink as well as random initial and boundary
91 conditions since the latter processes are known with uncertainties. The objectives of
92 this study are 1) to derive analytical solutions for the covariance, variance and
93 spectrum of groundwater level, and 2) to investigate the individual and combined
94 effects of these random processes on uncertainties and scaling of *h(x, t)*. In the
95 following we will first present the formulation and analytical solutions, then discuss
96 the results, and finally draw some conclusions.
97

98 ## 2. Formulation and Solutions

99 Under the Dupuit assumption, the one-dimensional transient groundwater flow in
100 an unconfined aquifer near a river (Fig. 1) can be approximated with the linearized
101 Boussinesq equation (Bear, 1972) with the initial and boundary conditions, i.e.,

102 $$T\frac{\partial^2 h}{\partial x^2}+W(t)=S_Y\frac{\partial h}{\partial t} \qquad (1a)$$

103 $$h(x,t)_{|t=0}=H_0(x); \qquad T\frac{\partial h}{\partial x}\bigg|_{x=0}=Q(t); \qquad h(x,t)|_{x=L}=H(t) \qquad (1b)$$

104 where T [L/T] is the transmissivity, h [L] is the hydraulic head or groundwater level
105 above the bottom of the aquifer which is assumed to be horizontal, $W(t)$ [L/T] is the
106 time-dependent source/sink term representing areal recharge or evapotranspiration, S_Y

is the specific yield, $H_0(x)$ [L] is the initial condition, *Q(t)* [L²/T] is the time-dependent flux at the left boundary, *H(t)* [L] is the time-dependent water level at the right boundary, *L* [L] is distance from the left to the right boundary, *x* [L] is the coordinate, and *t* [T] is time. In this study the initial head $H_0(x)$ is taken to be a spatially random variable, and the source/sink, *W(t)*, the flux to the left boundary, *Q(t)*, and the head at the right boundary, *H(t)*, are all taken to be temporally random processes and spatially deterministic. The parameters T and S_Y are taken to be constant.

The groundwater level, *h(x, t)*, the three random processes, *W(t)*, *Q(t)*, and *H(t)*, and the random variable, $H_0(x)$, are expressed in terms of their respective ensemble means plus small perturbations,

$$h(x,t) = \langle h(x,t) \rangle + h'(x,t) \tag{2a}$$

$$W(t) = \langle W(t) \rangle + W'(t); \qquad Q(t) = \langle Q(t) \rangle + Q'(t) \tag{2b}$$

$$H(t) = \langle H(t) \rangle + H'(t); \qquad H_0(x) = \langle H_0(x) \rangle + H_0'(x) \tag{2c}$$

where < > stands for ensemble average and ' for perturbation. ~~Although the~~The initial condition $H_0(x)$ in (1) can be any function. For the conceptualization of the groundwater flow presented in Fig. 1, the steady-state condition can be reached in ~~an~~this aquifer after a rainfall or during a wet season. Thus the steady-state solution to ~~initial head~~ this model were often adopted as initial condition in previous research (Liang and Zhang, 2012, 2013a, b). Thus, in this study, ~~, it is appropriate to~~ we set ~~it~~ initial condition $H_0(x)$ to be the steady-state solution to the one-dimensional ~~transient~~ groundwater flow equation, i.e., $H_0(x) = h_0 + 0.5W_0(L^2 - x^2)/T$, where h_0 [L] is the constant groundwater level at the right boundary and W_0 [L/T] is the spatially constant recharge rate (Liang and Zhang, 2012). Since h_0 is taken to be constant, the

带格式的: 字体: Times New Roman
带格式的: 字体: Times New Roman
带格式的: 字体: 非倾斜
带格式的: 字体: Times New Roman, 小四
带格式的
带格式的: 字体: (中文) 宋体
带格式的: 字体: Times New Roman, 小四
带格式的: 字体颜色: 红色

source of the uncertainty in the initial head $H_0(x)$ is due to random W_0 only. Thus, the mean and perturbation of $H_0(x)$ can be written as, $\langle H_0(x)\rangle = h_0 + 0.5\langle W_0\rangle(L^2 - x^2)/T$ and $H_0'(x) = 0.5W_0'(L^2 - x^2)/T$, respectively. By substituting Eq. (2), $\langle H_0(x)\rangle$, and $H_0'(x)$ into Eq. (1) and taking expectation, one obtains the mean flow equation with the mean initial and boundary conditions as

带格式的：字体颜色：红色

带格式的：字体颜色：红色

$$T\frac{\partial^2\langle h\rangle}{\partial x^2} + \langle W\rangle = S_Y\frac{\partial\langle h\rangle}{\partial t} \tag{3a}$$

$$\langle h(x,0)\rangle = h_0 + \frac{\langle W_0\rangle}{2T}(L^2 - x^2);\quad T\frac{\partial\langle h\rangle}{\partial x}\Big|_{x=0} = \langle Q\rangle;\quad \langle h(L,t)\rangle = \langle H(t)\rangle \tag{3b}$$

Subtracting Eq. (3) from (1) leads to the following perturbation equation with the initial and boundary conditions

$$T\frac{\partial^2 h'}{\partial x^2} + W' = S_Y\frac{\partial h'}{\partial t} \tag{4a}$$

$$h'(x,0) = \frac{W_0'}{2T}(L^2 - x^2);\quad T\frac{\partial h'}{\partial x}\Big|_{x=0} = Q';\quad h'(L,t) = H'(t) \tag{4b}$$

The analytical solution to Eq. (4) can be derived with integral-transform methods (Ozisik, 1968) given by

$$h' = \frac{2}{L}\sum_{n=0}^{\infty} e^{-\beta b_n^2 t}\cos(b_n x)\left[\frac{(-1)^n}{b_n^3 T}W_0' + \beta\int_0^t e^{\beta b_n^2\xi}\left[\frac{(-1)^n}{Tb_n}W'(\xi) - \frac{Q'(\xi)}{T} + H'(\xi)(-1)^n b_n\right]d\xi\right] \tag{5}$$

where $\beta = T/S_Y$, $b_n = (2n+1)\pi/(2L)$. Using Eq. (5), the temporal covariance of the groundwater level fluctuations can be derived as

$$\begin{aligned} C_{hh}(x,t_1;x,t_2) &= E[h'(x,t_1)h'(x,t_2)] \\ &= \frac{4}{L^2}\sum_{m=0}^{\infty}\sum_{n=0}^{\infty} e^{-\beta\left(b_m^2 t_1 + b_n^2 t_2\right)}\cos(b_m x)\cos(b_n x)\left[\frac{(-1)^{m+n}}{T^2 b_m^3 b_n^3}\sigma_{W_0}^2\right. \\ &\left. + \beta^2\int_0^{t_1}\int_0^{t_2} e^{\beta\left(b_m^2\xi + b_n^2\rho\right)}\left[\frac{(-1)^{n+m}}{T^2 b_m b_n}C_{WW}(\xi,\rho) + \frac{C_{QQ}(\xi,\rho)}{T^2} + C_{HH}(\xi,\rho)(-1)^{m+n}b_m b_n\right]d\xi d\rho\right] \end{aligned} \tag{6}$$

in which $\sigma_{W_0}^2$ is the variance of W_0, and $C_{WW}(\xi,\rho), C_{QQ}(\xi,\rho)$ and $C_{HH}(\xi,\rho)$ are the temporal auto-covariance of *W(t)*, of *Q(t)*, and *H(t)*, respectively. We assume that *W(t)*, Q*(t)*, and *H(t)* are uncorrelated in order to simplify our analyses. It is shown in Eq. (6) that the head covariance depends on the variance of W_0 and the covariances of *W(t)*, Q*(t)*, and *H(t)* and this equation can be evaluated for any random *W(t)*, Q*(t)*, and *H(t)*. We assume that these processes are white noises as employed in previous studies (Gelhar, 1993;Hantush and Marino, 1994;Liang and Zhang, 2013a). More realistic randomness of these processes will be considered in future studies.

Following *Gelhar* (1993, p.34), we express the spectra of *W(t)*, Q*(t)*, and *H(t)* as $S_{WW}=\sigma_W^2\lambda_W/\pi$, $S_{QQ}=\sigma_Q^2\lambda_Q/\pi$, and $S_{HH}=\sigma_H^2\lambda_H/\pi$, respectively, where σ_W^2, σ_Q^2, and σ_H^2 are the variances and λ_W, λ_Q, and λ_H are the correlation time intervals of these three processes, respectively. The corresponding covariance of *W(t)*, *Q(t)* and *H(t)* are $C_{WW}(\xi,\rho)=2\sigma_W^2\lambda_W\delta(\xi-\rho)$, $C_{QQ}(\xi,\rho)=2\sigma_Q^2\lambda_Q\delta(\xi-\rho)$, and $C_{HH}(\xi,\rho)=2\sigma_H^2\lambda_H\delta(\xi-\rho)$. Substituting these covariance into (6) and taking integration, one obtain analytical solution of head covariance

$$C_{hh}(x',t',\tau')=\frac{4\beta L^2}{T^2}\sum_{m=0}^{\infty}\sum_{n=0}^{\infty}\cos(b'_m x')\cos(b'_n x')\left\{e^{-\left[\left(b'^2_m+b'^2_n\right)t'+\left(b'^2_n-b'^2_m\right)\frac{\tau'}{2}\right]}\frac{L^2(-1)^{m+n}\sigma_{W_0}^2}{\beta b'^3_m b'^3_n}\right.$$
$$\left.+2\frac{\left(e^{-b'^2_m\tau'}-e^{-2b'^2_m t'}\right)}{\left(b'^2_m+b'^2_n\right)}\left[\frac{(-1)^{m+n}\sigma_W^2\lambda_W}{b'_m b'_n}+\frac{\sigma_Q^2\lambda_Q}{L^2}+\frac{(-1)^{m+n}b'_m b'_n T^2\sigma_H^2\lambda_H}{L^4}\right]\right\} \quad (7)$$

where $\tau'=t'_2-t'_1$ and $t'=(t'_2+t'_1)/2$. The analytical solution for the head variance can be obtain by setting $\tau'=0$

$$\sigma_h^2(x',t')=\frac{4\beta L^2}{T^2}\sum_{m=0}^{\infty}\sum_{n=0}^{\infty}\cos(b'_m x')\cos(b'_n x')\left\{e^{-\left(b'^2_m+b'^2_n\right)t'}\frac{L^2}{\beta}\frac{(-1)^{m+n}\sigma_{W_0}^2}{b'^3_m b'^3_n}+\right.$$
$$\left.2\frac{1-e^{-2b'^2_m t'}}{\left(b'^2_m+b'^2_n\right)}\left[\frac{(-1)^{m+n}\sigma_W^2\lambda_W}{b'_m b'_n}+\frac{\sigma_Q^2\lambda_Q}{L^2}+\frac{(-1)^{m+n}b'_m b'_n T^2\sigma_H^2\lambda_H}{L^4}\right]\right\} \quad (8)$$

where

$$t'=\frac{t}{t_c};\quad x'=\frac{x}{L};\quad t_c=\frac{L^2}{\beta};\quad b'_n=\frac{(2n+1)\pi}{2}$$

in which $t_c(=S_Y L^2/(KM))$ [1/T] is a characteristic timescale (Gelhar, 1993) where the transmissivity (T) is replaced by the product of the hydraulic conductivity (K) and the average saturated thickness (M) of the aquifer. The characteristic timescale (t_c) is an important parameter and its value for most shallow aquifers is usually larger than 100 day since the horizontal extent of a shallow aquifer is usually much larger than its thickness. For instance, the value of t_c is 250 days for a sandy aquifer with L=100m, M =10m, K=1m/day, and S_Y=0.25.

The spectral density of *h(x, t)* can't be derived by ordinary Fourier transform since the head covariance and variance depend on time *t'* and thus *h(x, t)* are temporally non-stationary as shown in Eqs. (7) and (8). Priestley (1981) defined the spectral density of non-stationary processes (Wigner spectrum) as the Fourier transform of time-dependent auto-covariance with fixed reference time *t* and derived time-dependent spectral density. In order to obtain the spectrum of *h(x, t)*, we applied Priestley's method and obtained the time-dependent spectral density (Priestley, 1981; Zhang and Li, 2005;Liang and Zhang, 2013a), i.e.,

$$S_{hh}(x,t,\omega)=\frac{1}{2\pi}\int_{-\infty}^{\infty}C_{hh}(x,t,\tau)e^{-i\omega\tau}d\tau$$
$$=\sum_{m=0}^{\infty}\sum_{n=0}^{\infty}\cos(b_m x)\cos(b_n x)\frac{2t_c\left(b_n^2-b_m^2\right)e^{-\beta\left(b_m^2+b_n^2\right)t}}{\beta^2\left(b_n^2-b_m^2\right)^2/4+\omega^2}\frac{(-1)^{m+n}\sigma_{W_0}^2}{\pi T^2 b_m^3 b_n^3}+ \quad (9)$$
$$\sum_{m=0}^{\infty}\sum_{n=0}^{\infty}\cos(b_m x)\cos(b_n x)\frac{8\beta b_m^2}{t_c\left(b_m^2+b_n^2\right)}\frac{1}{\beta^2 b_m^4+\omega^2}\left[\frac{(-1)^{m+n}S_{WW}}{T^2 b_m b_n}+\frac{S_{QQ}}{T^2}+(-1)^{m+n}b_m b_n S_{HH}\right]$$

where ω is angular frequency and $\omega = 2\pi f$, f is frequency, and $i = \sqrt{-1}$. It is seen in Eq. (9) that the spectrum S_{hh} is dependent on not only frequency and locations but also time t. The time-dependent term (i.e., first term) in Eq. (9) is caused by the random initial condition and is proportional to $e^{-\beta\left(b_m^2+b_n^2\right)t}$ which decays quickly with t. We evaluated the first term in the Eq. (9) by setting t=0 and found that it is much smaller than the second term in Eq. (9). We thus ignored the first term and evaluated the spectrum using the approximation,

$$S_{hh}(x',\omega)=\sum_{m=0}^{\infty}\sum_{n=0}^{\infty}\frac{8\beta b'^2_m\cos(b'_m x')\cos(b'_n x')}{t_c\left(b'^2_m+b'^2_n\right)\left(\beta^2 b'^4_m/L^4+\omega^2\right)}\left[\frac{(-1)^{m+n}S_{WW}L^2}{T^2 b'_m b'_n}+\frac{S_{QQ}}{T^2}+\frac{(-1)^{m+n}b'_m b'_n S_{HH}}{L^2}\right] \quad (10)$$

3. Results and Discussion

3.1 Variance of groundwater levels

The general expression of the head variance in Eq. (8) depends on the variances of the four random processes, $\sigma^2_{W_0}$, σ^2_W, σ^2_Q, and σ^2_H. In the following we will study their individual and combined effects on the head variation and focus our attention only on the variance of $h(x, t)$. The dimensionless standard deviation of $h(x, t)$, σ'_h, or the square root of the dimensionless variance (σ'^2_h) as a function of the dimensionless time (t') were evaluated and presented in the left column of Fig. 2 at fixed dimensionless locations (x'). The σ'_h as a function of x' was evaluated and presented in the right column of Fig. 2 at fixed t'.

We first evaluate the effect of the random initial condition due to the random term, W_0, by setting ~~the variances of $W(t)$, $Q(t)$ and $H(t)$ to be zero, i.e.,~~ $\sigma^2_W = \sigma^2_Q = \sigma^2_H = 0$. In this case the dimensionless variance in Eq. (8) reduces to

带格式的：字体：倾斜
带格式的：非升高量 / 降低量
带格式的：非升高量 / 降低量
带格式的：字体：倾斜，非升高量 / 降低量
带格式的：非升高量 / 降低量
带格式的：非升高量 / 降低量
带格式的：字体：倾斜

$$\sigma'^{2}_{h}(x',t') = \sum_{m=0}^{\infty}\sum_{n=0}^{\infty} \frac{(-1)^{m+n}}{b'^{3}_{m}\, b'^{3}_{n}} \cos(b'_{m}\, x')\cos(b'_{n}\, x') e^{-\left(b'^{2}_{m}+b'^{2}_{n}\right)t'} \quad (11)$$

where $\sigma'^{2}_{h} = \sigma^{2}_{h} T^{2}/(4L^{4}\sigma^{2}_{W_0})$. ~~The~~ The changes of the ~~dimensionless standard deviation of $h(x, t)$, σ'_h ;~~ with x' and t' were presented in Fig 2a and 2b, respectively~~.or the square root of the dimensionless variance (σ'^{2}_{h}) in Eq. (11) as a function of the dimensionless time (t') was evaluated and presented in Fig. 2a. 1a at five dimensionless locations, x' = 0, 0.2, 0.4, 0.6, and 0.8.~~ It is shown in Fig. ~~1a~~ 2a that for a fixed location the ~~standard deviation~~ σ'_h is at its maximum at t'=0 and decreases with time gradually to a negligible number at t'=1.0. This means that the error in $h(x, t)$ predicted by an analytical or numerical solution due to the uncertain initial condition is significant at early time, especially near a flux boundary. The time duration during which the effect of the uncertain initial condition is significant depends on the value of the characteristic timescale (t_c) since $t'=t/t_c$. In the most aquifers this duration may last many days. In the typical aquifer studied ~~with L=100m, M =10m, K=1m/day, and S_s=0.25~~ the effect of the uncertainty in initial condition on $h(x, t)$ is significant during first 250 days (t'=1.0). This duration should be relatively short, however, in a more permeable aquifer whose horizontal extent (L) is relatively smaller than its thickness (M). ~~The dimensionless standard deviation (σ'_h) based on Eq. (11) as a function of the dimensionless location (x') was presented in Fig. 1b 2b for five dimensionless times, t' = 0.0, 0.2, 0.4, 0.6, and 0.8.~~ It is seen in Fig. ~~1b~~ 2b that for a fixed time， the σ'_h is the largest at the left flux boundary (x'=~~-~~0.0) and becomes zero at the right constant head boundary (x'=1.0)

带格式的：字体：倾斜
带格式的：字体：倾斜

since the right boundary is ~~known~~deterministic. This means that the error in *h(x, t)* predicted by an analytical or numerical solution due to the uncertain initial condition is significant almost everywhere in the aquifer: the further away from a constant head boundary ~~or the closer to a flux boundary~~, the larger the error.

We then consider the uncertainty in the areal source/sink term (*W*) by setting $\sigma_{W_0}^2 = \sigma_Q^2 = \sigma_H^2 = 0$. In this case the dimensionless variance in Eq. (8) reduces to

$$\sigma'^2_h(x',t') = 2\sum_{m=0}^{\infty}\sum_{n=0}^{\infty}\cos(b'_m x')\cos(b'_n x')\frac{(1-e^{-2b'^2_m t'})(-1)^{m+n}}{(b'^2_m+b'^2_n)b'_m b'_n} \qquad (12)$$

where $\sigma'^2_h = \sigma_h^2 TS_Y/(4L^2\sigma_W^2\lambda_W)$. The changes of the σ'_h with *x'* and *t'* were presented in Fig 2c and 2d, respectively. ~~The dimensionless standard deviation (σ'_h) based σ'^2_h in Eq. (12) as a function of the dimensionless time (*t'*) for the same five locations, *x'*=0.0, 0.2, 0.4, 0.6, and 0.8, was presented in Fig. 1c~~2c~~.~~ It is noticed in Fig. 2c that at a fixed location, the σ'_h is zero initially, gradually increases as time goes, and approaches a constant limit at later time. This means that the error in *h(x, t)* due to an source/sink is at its minimum at early time and increases with time to approach a constant limit at later time: the closer to the left flux boundary, the larger the limit. ~~The dimensionless standard deviation (σ'_h) versus the dimensionless location (x') for the dimensionless time, *t'*=0.0, 0.2, 0.4, 0.6, and 0.8, is presented in Fig. 1d~~2d~~.~~ For a fixed time the σ'_h decreases smoothly from the left to the right boundary (Fig. 2d). The error in *h(x, t)* due to the uncertainty in the source/sink is significant almost everywhere in the aquifer: the further away from the constant head boundary ~~or the closer to a flux boundary~~, the larger the error, similar to the previous case with the random initial condition (Fig. ~~1b~~2b).

Thirdly, we investigate the effect of the left random flux boundary by setting $\sigma_{W_0}^2 = \sigma_W^2 = \sigma_H^2 = 0$ in Eq. (8). In this case the dimensionless head variance is given by

$$\sigma'^2_h(x',t') = 2\sum_{m=0}^{\infty}\sum_{n=0}^{\infty}\cos(b'_m x')\cos(b'_n x')\frac{1-e^{-2b'^2_m t'}}{b'^2_m + b'^2_n} \qquad (13)$$

where $\sigma'^2_h = \sigma_h^2 TS_Y/(4\sigma_Q^2\lambda_Q)$. The changes of the σ'_h with x' and t' were presented in Fig 2e and 2f, respectively. ~~The dimensionless standard deviation (σ'_h) based on Eq. (13) as a function of the dimensionless time (t') is plotted in Fig. 1e 2e for x'=0.0, 0.2, 0.4, 0.6 and 0.8. Similar to the case of the random source/sink in Fig. 1c 2c, a~~At any location the σ'_h in Fig. ~~1e~~ 2e or the error in $h(x, t)$ due to an uncertain flux boundary is at its minimum at early time and increases quickly with time to approach a constant limit: the closer to the left flux boundary, the larger the limit. ~~The dimensionless deviation (σ'_h) as a function of the dimensionless location (x') is plotted in Fig. 1f 2f for t'=0.01, 0.1, and 1.0.~~ At any time the σ'_h in ~~this case~~ Fig. 2f or the error in the head due to the uncertain flux boundary is at its maximum at the left boundary but decreases quickly away from the boundary to become insignificant for x'>0.8.

Fourthly, we investigated the effect of the random head boundary by setting $\sigma_{W_0}^2 = \sigma_W^2 = \sigma_Q^2 = 0$ in Eq. (8). The dimensionless head variance in this case is given by

$$\sigma'^2_h(x',t') = 2\sum_{m=0}^{\infty}\sum_{n=0}^{\infty}\cos(b'_m x')\cos(b'_n x')\frac{(-1)^{m+n}b'_m b'_n\left(1-e^{-2b'^2_m t'}\right)}{\left(b'^2_m + b'^2_n\right)} \qquad (14)$$

where $\sigma'^2_h = \sigma_h^2 L^2 S_Y / (4T\sigma_H^2 \lambda_H)$. The changes of this σ'_h with *x'* and *t'* were presented in Fig 2g and 2h, respectively. ~~The dimensionless standard deviation (σ'_h) based on Eq. (14) as a function of the dimensionless time (*t'*) is provided in Fig. 1g 2g for *x'*=0.0, 0.2, 0.4, 0.6, and 0.8.~~ It seen in Fig. 2g that ~~Similar to the case of the random flux boundary (Fig. 1e2e), a~~at any location the σ'_h or the error in *h(x, t)* due to the random head boundary increases with time quickly to approach a constant limit: the closer to the uncertain head boundary, the larger the error. The spatial variation of σ'_h can be clearly observed in Fig. ~~1h~~ 2h for ~~t'=0.01, 0.1, and 1.0~~fixed *t'*. At any time σ'_h is at its maximum at the right boundary (*x'*=1) where the head is uncertain, decreases quickly away from the boundary. The error in *h(x, t)* due to the uncertain head boundary is limited in a narrow zone near the boundary (*x'*>0.8) (Fig. ~~1h~~2h).

带格式的：字体：非倾斜

带格式的：字体：非倾斜

Finally, we consider the combined effects of the uncertainties from all four sources, i.e., the initial condition, sources, and flux and head boundaries. The head variance in Eq. (8) is written in the dimensionless form as

$$\sigma'^2_h(x',t') = \sum_{m=0}^{\infty}\sum_{n=0}^{\infty}\cos(b'_m x')\cos(b'_n x')\left\{e^{-(b'^2_m+b'^2_n)t'}\frac{(-1)^{m+n}\sigma'^2_{W_0}}{b'^3_m b'^3_n} + 2\frac{1-e^{-2b'^2_m t'}}{(b'^2_m+b'^2_n)}\left[\frac{(-1)^{m+n}}{b'_m b'_n}+\sigma'^2_Q+(-1)^{m+n}b'_m b'_n \sigma'^2_H\right]\right\} \quad (15)$$

where

$$\sigma'^2_h = \frac{\sigma_h^2 T S_Y}{4L^2\sigma_W^2\lambda_W};\ \sigma'^2_{W_0} = \frac{L^2 S_Y \sigma^2_{W_0}}{T\sigma_W^2\lambda_W};\ \sigma'^2_Q = \frac{\sigma_Q^2\lambda_Q}{L^2\sigma_W^2\lambda_W};\ \sigma'^2_H = \frac{T^2\sigma_H^2\lambda_H}{L^4\sigma_W^2\lambda_W}$$

The dimensionless variances, $\sigma'^2_{W_0}$, σ'^2_Q and σ'^2_H, need to be specified in order to evaluate the dimensionless $\sigma'^2_h(x',t')$ in Eq. (15). For the typical aquifer mentioned above with L=100m, T=10 m^2/day (or K=1m/day and M=10m) and S_Y=0.25, we set $\sigma^2_{W_0}/(\sigma^2_W\lambda_W)=10^{-1}$, $\sigma^2_Q\lambda_Q/(\sigma^2_W\lambda_W)=10^3$, $\sigma^2_H\lambda_H/(\sigma^2_W\lambda_W)=10^4$ and obtain $\sigma'^2_{W_0}=25$, $\sigma'^2_Q=0.1$ and $\sigma'^2_H=0.01$.

The changes of this σ'_h with *x'* and *t'* were presented in Fig 2i and 2j, respectively. ~~The dimensionless standard deviation (σ'_h) based on Eq. (15) as a function of the dimensionless time (*t'*) is presented in Fig. 2a~~ 2i ~~for *x'*=0.0, 0.2, 0.4, 0.6, and 0.8.~~ It is observed in Fig. ~~2a~~ 2i that at any location the σ'_h is at its maximum due to the uncertainty in the initial condition, gradually decreases as time goes, and approaches a constant limit at later time (*t'*>0.6) which is due to the combined effects of the uncertain source/sink and flux and head boundaries. This means that the error in the head in early time is significant if the initial condition is uncertain and reduces as time goes to reach a constant limit ~~or error in later time~~. The error in head in later time is determined by the uncertainties in the source/sink, flux and head boundaries. ~~The spatial variation of the dimensionless standard deviation (σ'_h) for this case is provided in Fig. 2b~~ 2j ~~for *t'*=0.01, 0.2, 0.4, 0.6, and 0.8.~~ It can be observed in Fig. 2j that σ'_h is relatively larger near both boundaries. The values of σ'_h at the two boundaries are equivalent (~1.3) at early time, say *t'*=0.01 (the top curve in Fig. ~~2b~~2j) and it reduces slowly away from the flux boundary but quickly away from the head boundary. As time progresses, the σ'_h near the head boundary stays more or less the same but reduces significantly in

most part of the aquifer. This means that in early time the error in *h(x, t)* in most part of the aquifer is mainly caused by the initial condition and at later time it is due to the combined effects of the uncertain areal source/sink and flux boundary. The effect of the uncertain head boundary on *h(x, t)* doesn't change with time significantly but is limited in a narrow zone near the boundary.

3.2 Spectrum of groundwater levels

We first evaluated S_{hh} in Eq. (10) due to the effect of the white noise flux boundary only by setting $S_{QQ} \neq 0$, $S_{WW} = 0$, and $S_{HH} = 0$. The dimensionless spectrum S_{hh}/S_{QQ} as a function of the frequency (*f*) was evaluated and presented in the log-log plot (Fig. 3a-3c) for three values of t_c (40, 400, and 4,000 days) since the value of t_c is 250 days for a sandy aquifer ~~with L=100m, M =10m, K=1m/day, and S_y=0.25~~ as we mentioned above and at the six locations (*x'* = 0.0, 0.2, 0.4, 0.6, 0.8, and 0.9). The spectrum S_{hh}/S_{QQ} in Fig. 3a is more or less horizontal (i.e., white noise) at low frequencies and decrease gradually as *f* increases, indicating that an aquifer acts as a low-bass filter that filter signals at high frequencies and keep signals at low frequencies. The aquifer has significantly dampened the fluctuations of the groundwater level. The spectrum varies with the location *x'*: the smaller the value of *x'* or the closer to the left flux boundary (*x'*=0), the larger the spectrum (Fig. 3a-3c). All spectra in Fig. 3a are not a straight line in the log-log plot, meaning that the temporal scaling of *h(x, t)* doesn't exist in the range of $f = 10^{-3} \sim 10^{0}$ when t_c=40 days. As t_c increases to 400 and 4000 days, however, the spectrum at *x'*=0 become a straight line (the top curve in Fig. 3b and 3c) or has a power-law relation with *f*, i.e.,

$S_{hh}/S_{QQ} \propto 1/f$, since its slope is approximately one. The fluctuations of *h(0, t)* is a pink noise due to the white noise fluctuations flux boundary when the characteristic timescale (t_c) is large which means that the aquifer is relatively less permeable and/or has a much larger horizontal length than its thickness.

Secondly, the spectrum S_{hh}/S_{HH} due to the sole effect of the random head boundary was evaluated by setting $S_{HH} \neq 0$, $S_{WW} = 0$, and $S_{QQ} = 0$ in Eq. (10) for the same three values of t_c and six locations and presented in Fig. 3d-3f as a function of *f*. It is shown that similar to Fig. 3a-3c, the spectrum decreases as *f* increases but different from Fig. 3a-3c, the spectrum is larger at *x'*=0.9 near the right boundary (the top curves in Fig. 3d-3f) than that *x'*=0.0 (the bottom curves). Furthermore, none of the spectra are a straight line in the log-log plot, indicating that the temporal scaling of groundwater level fluctuations doesn't exist in the case of the white noise head boundary.

Thirdly, the spectrum S_{hh}/S_{WW} due the effect of the white noise recharge only was evaluated by setting $S_{WW} \neq 0$, $S_{QQ} = 0$, and $S_{HH} = 0$ in Eq. (10) for the same values of t_c and *x'* and presented in Fig. 3g-3i as a function of *f*. It is shown that when t_c=40 day the spectrum in Fig. 3g is horizontal at low frequencies and become a straight line at high frequencies: the closer to the right head boundary, the later it approaches a straight line (Fig. 3h). As t_c increases to 400 and 4000 days, the slope of the spectrum at all locations except at *x'*=0.9 approaches to a straight line with a slope of 2 (Fig. 3h and 3i), indicating a temporal scaling of *h(x, t)*. The fluctuations of groundwater level is a Brownian motion, i.e., $S \propto 1/f^2$, when $t_c \geq 4000$ day or in

a relatively less permeable and/or has a much larger horizontal length than its thickness.

Finally, the head spectrum due to the combined effect of all three random sources (the white noise recharge, and flux and head boundaries) was evaluated, i.e., $S_{WW} \neq 0$, $S_{QQ} \neq 0$, and $S_{HH} \neq 0$ in Eq. (10). The spectrum of S_{hh}/S_{WW} as a function of f was presented in Fig. ~~4~~3j-3l for the same values of t_c and x' where $S_{QQ}/S_{WW} = 1000$ and $S_{HH}/S_{WW} = 10000$ which are same with the values using in previous section. It is noticed that the general patterns of S_{hh}/S_{WW} in the combined case ~~(Fig. 4)~~ is similar to the case under the random source/sink only (Fig. 3g-3i) except at x'=0.0 and 0.9 (the dashed and dotted curves in Fig. ~~4a~~3j, respectively) due to the strong effects of the boundary conditions at these two locations. At t_c=4000 day, the spectra at all locations except x'=0.0 (Fig. ~~4c~~3l) are similar to those in Fig. 3i, indicating the dominating effect of the random areal source/sink. The spectrum at x'=0 in this case is also a straight line (the dashed curve in Fig. ~~4c~~3l) but with a different slope due to the effect of the random flux boundary which is similar to the top straight line in Fig. 3c. Above results provide a theoretical explanation as why temporal scaling exists in the observed groundwater level fluctuations (Zhang and Schilling, 2004;Bloomfield and Little, 2010;Zhu et al., 2012). We thus conclude that temporal scaling of *h(x, t)* may indeed exist in real aquifers due to the strong effect of the areal source/sink.

~~It is noted that the~~

4. Conclusions

In this study the effects of random source/sink, and initial and boundary conditions on the uncertainty and temporal scaling of the groundwater level, *h(x, t)* were investigated. The analytical solutions for the variance, covariance and spectrum of *h(x, t)* in an unconfined aquifer described by a linearized Boussinesq equation with white noise source/sink, and initial and boundary conditions were derived. The standard deviations of *h(x, t)* for various cases were evaluated. Based on the results, the following conclusions can be drawn.

1. The error in *h(x, t)* due to a random initial condition is significant at early time, especially near a flux boundary. The duration during which the effect is significant may last a few hundred days in most aquifers;

2. The error in *h(x, t)* due to a random areal source/sink is significant in most part of an aquifer: the closer to a flux boundary, the larger the error;

3. The errors in *h(x, t)* due to random flux and head boundaries are significant near the boundaries: the closer to the boundaries, the larger the errors. The random flux boundary may affect the head over a larger region near the boundary than the random head boundary;

4. In the typical sandy aquifer studied (with the length of aquifer at the direction of water flow L=100m, the average saturated thickness M =10m, hydraulic conductivity K=1m/day, and specific yield S_Y=0.25) the error in *h(x, t)* in early time is mainly caused by an uncertain initial condition and the error reduces as time goes to reach a constant error in later time. The constant error in *h(x, t)* is mainly due to the combined effects of uncertain source/sink and boundaries;

带格式的：缩进：左侧： 0 厘米，首行缩进： 1.77 字符

带格式的：字体：小四

带格式的：字体：小四

带格式的：字体：小四

5. The aquifer system behaves as a low-pass filter which filter the short-term (~~low~~ high frequencies) fluctuations and keep the long-term (low frequencies) fluctuations;

6. Temporal scaling of groundwater level fluctuations may indeed exist in most part of a low permeable aquifer whose horizontal length is much larger than its thickness caused by the temporal fluctuations of areal source/sink.

Finally, it is pointed out that the analyses carried out in this study is under the assumptions that the processes, *W(t)*, Q*(t)*, and *H(t)* are uncorrelated white noises. In reality, they may be correlated and spatially varied. We plan to relax those constrains and study more realistic cases in the near future. It is also noted that the analytical solutions for head variances derived in this study provide a way to identify and quantify the uncertainty. The spectrum relationship obtained among the head, recharge and boundary conditions can help one to improve spectrum analysis for a groundwater level time series and removed the effects of the boundary conditions.

Acknowledgment

This study was partially supported with the research grants from the National Nature Science Foundation of China (NSFC-41272260; NSFC-41330314; NSFC-41302180), the Natural Science Foundation of Jiangsu Province (SBK201341336) and from the National Key project "Water Pollution Control in the Huai River Basin" of China (2012ZX07204-001, 2012ZX07204-003).

References

Bear, J.: Dynamics of fluids in porous media, Environmental science series (New York, 1972-),

American Elsevier Pub. Co., New York,, xvii, 764 p. pp., 1972.
Beven, K., and Binley, A.: The Future of Distributed Models - Model Calibration and Uncertainty Prediction, Hydrol Process, 6, 279-298, 1992.
Bloomfield, J. P., and Little, M. A.: Robust evidence for random fractal scaling of groundwater levels in unconfined aquifers, J Hydrol, 393, 362-369, DOI 10.1016/j.jhydrol.2010.08.031, 2010.
Dagan, G.: Flow and transport in porous formations, Springer-Verlag, Berlin ; New York, xvii, 465 p. pp., 1989.
Gelhar, L. W.: Stochastic subsurface hydrology, Prentice-Hall, Englewood Cliffs, N.J., x, 390 p. pp., 1993.
Hantush, M. M., and Marino, M. A.: One-Dimensional Stochastic-Analysis in Leaky Aquifers Subject to Random Leakage, Water Resour Res, 30, 549-558, Doi 10.1029/93wr02887, 1994.
Liang, X. Y., and Zhang, Y. K.: A new analytical method for groundwater recharge and discharge estimation, J Hydrol, 450, 17-24, DOI 10.1016/j.jhydrol.2012.05.036, 2012.
Liang, X. Y., and Zhang, Y. K.: Temporal and spatial variation and scaling of groundwater levels in a bounded unconfined aquifer, J Hydrol, 479, 139-145, DOI 10.1016/j.jhydrol.2012.11.044, 2013a.
Liang, X. Y., and Zhang, Y. K.: Analytic solutions to transient groundwater flow under time-dependent sources in a heterogeneous aquifer bounded by fluctuating river stage, Adv Water Resour, 58, 1-9, DOI 10.1016/j.advwatres.2013.03.010, 2013b.
~~Liang, X. Y., and Zhang, Y. K.: A new analytical method for groundwater recharge and discharge estimation, J Hydrol, 450, 17-24, DOI 10.1016/j.jhydrol.2012.05.036, 2012.~~
~~Liang, X. Y., and Zhang, Y. K.: Temporal and spatial variation and scaling of groundwater levels in a bounded unconfined aquifer, J Hydrol, 479, 139-145, DOI 10.1016/j.jhydrol.2012.11.044, 2013.~~
Neuman, S. P.: Maximum likelihood Bayesian averaging of uncertain model predictions, Stoch Env Res Risk A, 17, 291-305, 10.1007/s00477-003-0151-7, 2003.
Neuman, S. P., Xue, L., Ye, M., and Lu, D.: Bayesian analysis of data-worth considering model and parameter uncertainties, Advances in Water Resources, 36, 75-85, 10.1016/j.advwatres.2011.02.007, 2012.
Nowak, W., de Barros, F. P. J., and Rubin, Y.: Bayesian geostatistical design: Task-driven optimal site investigation when the geostatistical model is uncertain, Water Resour Res, 46, Artn W03535 Doi 10.1029/2009wr008312, 2010.

Priestley, M. B.: Spectral Analysis and Time Series, Academic Press, San Diego, 1981.
Refsgaard, J. C., van der Sluijs, J. P., Hojberg, A. L., and Vanrolleghem, P. A.: Uncertainty in the environmental modelling process - A framework and guidance, Environmental Modelling & Software, 22, 1543-1556, 10.1016/j.envost.2007.02.004, 2007.
Rojas, R., Feyen, L., and Dassargues, A.: Conceptual model uncertainty in groundwater modeling: Combining generalized likelihood uncertainty estimation and Bayesian model averaging, Water Resources Research, 44, 10.1029/2008wr006908, 2008.
Rojas, R., Feyen, L., Batelaan, O., and Dassargues, A.: On the value of conditioning data to reduce conceptual model uncertainty in groundwater modeling, Water Resources Research, 46, 20, 10.1029/2009wr008822, 2010.
Schilling, K. E., and Zhang, Y. K.: Temporal Scaling of Groundwater Level Fluctuations Near a Stream, Ground Water, 50, 59-67, DOI 10.1111/j.1745-6584.2011.00804.x, 2012.

带格式的： 缩进：悬挂缩进：2.12 字符，左 0.01 字符，首行缩进： -2.12 字符

Vrugt, J. A., Gupta, H. V., Bouten, W., and Sorooshian, S.: A Shuffled Complex Evolution Metropolis algorithm for optimization and uncertainty assessment of hydrologic model parameters, Water Resources Research, 39, 10.1029/2002wr001642, 2003.

Ye, M., Meyer, P. D., and Neuman, S. P.: On model selection criteria in multimodel analysis, Water Resources Research, 44, 10.1029/2008wr006803, 2008.

Zeng, X. K., Wang, D., Wu, J. C., and Chen, X.: Reliability Analysis of the Groundwater Conceptual Model, Human and Ecological Risk Assessment, 19, 515-525, 10.1080/10807039.2012.713822, 2013.

Zhang, D.: Stochastic methods for flow in porous media : coping with uncertainties, Academic, San Diego, Calif. London, xiv, 350 p. pp., 2002.

Zhang, Y. K., and Schilling, K.: Temporal scaling of hydraulic head and river base flow and its implication for groundwater recharge, Water Resour Res, 40, -, Artn W03504 Doi 10.1029/2003wr002094, 2004.

Zhang, Y. K., and Li, Z. W.: Temporal scaling of hydraulic head fluctuations: Nonstationary spectral analyses and numerical simulations, Water Resources Research, 41, 10.1029/2004wr003797, 2005.

Zhang, Y. K., and Li, Z. W.: Effect of temporally correlated recharge on fluctuations of groundwater levels, Water Resources Research, 42, 10.1029/2005wr004828, 2006.

Zhang, Y. K., and Yang, X. Y.: Effects of variations of river stage and hydraulic conductivity on temporal scaling of groundwater levels: numerical simulations, Stoch Env Res Risk A, 24, 1043-1052, DOI 10.1007/s00477-010-0437-5, 2010.

Zhu, J. T., Young, M. H., and Osterberg, J.: Impacts of riparian zone plant water use on temporal scaling of groundwater systems, Hydrol Process, 26, 1352-1360, Doi 10.1002/Hyp.8241, 2012.

Figure captions

Figure 1 A schematic of the unconfined aquifer studied where $W(t)$ is the random time-dependent source/sink, $H_0(x)$ is the random initial condition, $Q(t)$ is the random time-dependent flux at the left boundary, $H(t)$ is the random time-dependent water level at the right boundary, L is distance from the left to the right boundary, and $h(x, t)$ is the random groundwater level in the aquifer.

Figure 2 The graphs on the left column are the standard deviation (σ'_h) of groundwater level ($h(x, t)$) versus the dimensionless time (t') at the dimensionless locations x'=0.0, 0.2, 0.4, 0.6, and 0.8. The graphs on the right column are σ'_h versus x' for the different t': b) and d) are for t'= 0.0, 0.2, 0.4, 0.6 and 0.8, f) and h) are for t'=0.01, 0.1, and 1.0, and j) is for t'=0.01, 0.2, 0.4, 0.6 and 0.8. Also, a) and b) are based on Eq.(11) where $\sigma_W^2 = \sigma_Q^2 = \sigma_H^2 = 0$; c) and d) are based on Eq. (12) where $\sigma_{W_0}^2 = \sigma_Q^2 = \sigma_H^2 = 0$; e) and f) are based on Eq. (13) where $\sigma_{W_0}^2 = \sigma_W^2 = \sigma_H^2 = 0$; g) and h) are based on Eq. (14) where $\sigma_{W_0}^2 = \sigma_W^2 = \sigma_Q^2 = 0$; i) and j) are based on Eq.(15) where $\sigma_{W_0}^2 \neq \sigma_W^2 \neq \sigma_Q^2 \neq \sigma_H^2 \neq 0$.

Figure 3 The dimensionless power spectrum versus frequency (f) at the dimensionless locations x'=0.0, 0.2, 0.4, 0.6, 0.8, and 0.9. The graphs on the left column are for t_c = 40 day, the graphs on the middle column are for t_c = 400 day, and the graphs on the right column are for t_c = 4000 day. The graphs on the first row are the dimensionless spectrum S_{hh}/S_{QQ} when $S_{WW} = 0$, $S_{HH} = 0$, and $S_{QQ} \neq 0$ in Eq. (10), the graphs on the second row is S_{hh}/S_{HH} when $S_{WW} = 0$, $S_{QQ} = 0$, and $S_{HH} \neq 0$, the graphs on the third row are S_{hh}/S_{WW} when $S_{QQ} = 0$, $S_{HH} = 0$, and $S_{WW} \neq 0$, and the graphs on the bottom row is S_{hh}/S_{WW} when $S_{QQ} \neq 0$, $S_{HH} \neq 0$, and $S_{WW} \neq 0$.

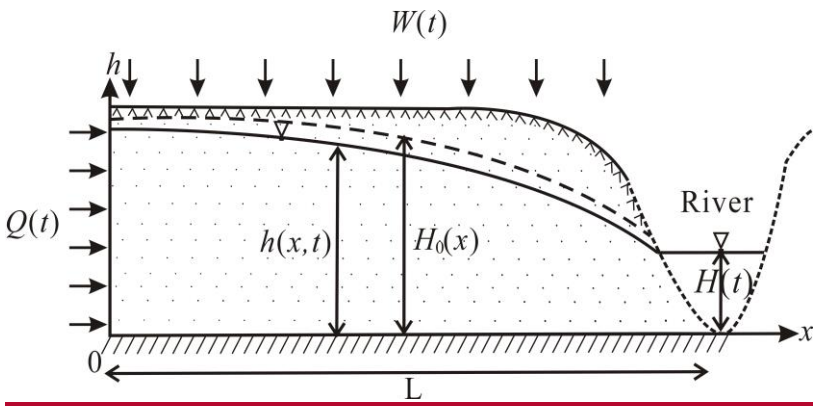

516

517 **Figure 1**

518

519

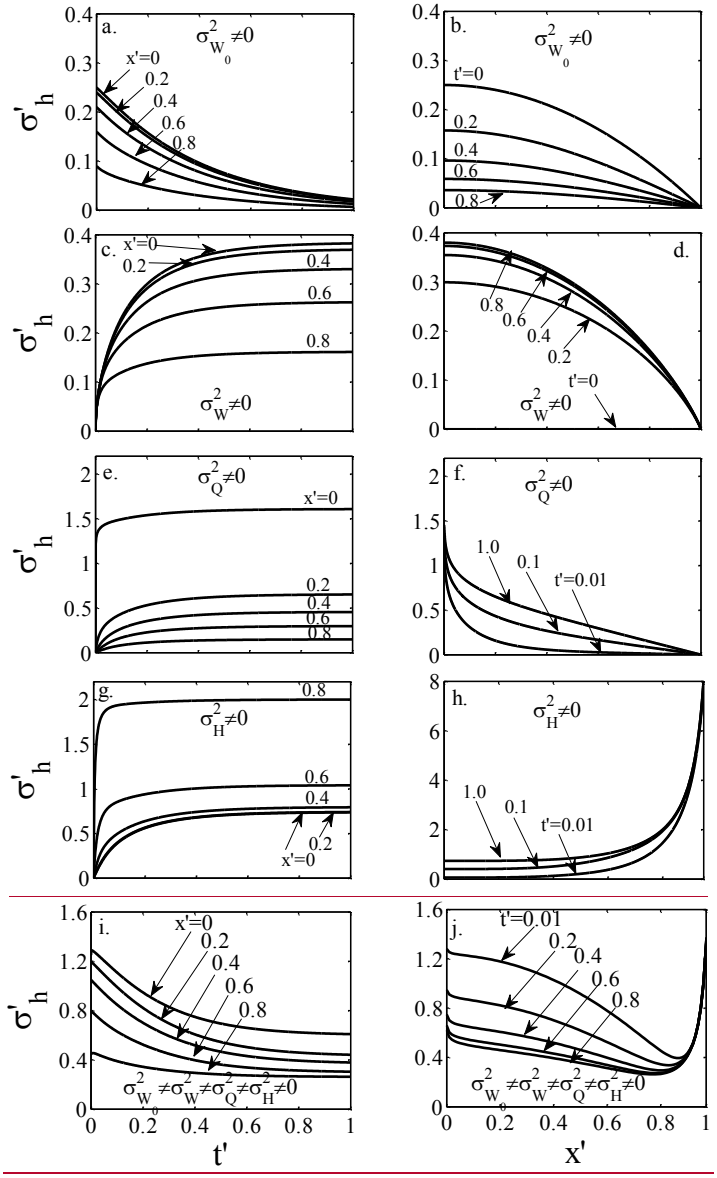
a.
$\sigma^2_{W_0}\neq 0$
x'=0
0.2
0.4
0.6
0.8
b.
$\sigma^2_{W_0}\neq 0$
t'=0
0.2
0.4
0.6
0.8
c.
x'=0
0.2
0.4
0.6
0.8
$\sigma^2_W\neq 0$
d.
0.8
0.6
0.4
0.2
t'=0
$\sigma^2_W\neq 0$
e.
$\sigma^2_Q\neq 0$
x'=0
0.2
0.4
0.6
0.8
f.
$\sigma^2_Q\neq 0$
1.0
0.1
t'=0.01
g.
0.8
$\sigma^2_H\neq 0$
0.6
0.4
0.2
x'=0
h.
$\sigma^2_H\neq 0$
1.0
0.1
t'=0.01
i.
x'=0
0.2
0.4
0.6
0.8
$\sigma^2_{W_0}\neq\sigma^2_W\neq\sigma^2_Q\neq\sigma^2_H\neq 0$
j.
t'=0.01
0.2
0.4
0.6
0.8
$\sigma^2_{W_0}\neq\sigma^2_W\neq\sigma^2_Q\neq\sigma^2_H\neq 0$
σ'h
t'
x'

Figure 2

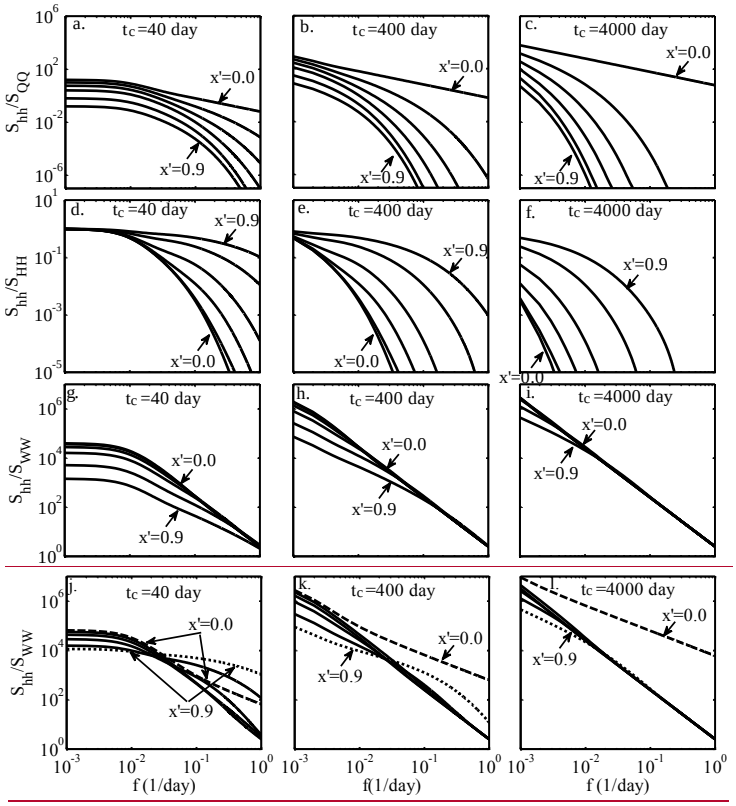

Figure 3

~~Figure captions~~

~~**Figure 1** A schematic of the unconfined aquifer studied where W(t) is the time-dependent random source/sink, $H_0(x)$ is the random initial condition, Q(t) is the random time-dependent flux at the left boundary, H(t) is the random time-dependent water level at the right boundary, L [L] is distance from the left to the right boundary, and h(x, t) is the random groundwater level in the aquifer.~~

~~**Figure 2** The graphs on the left column (five graphs) are the standard deviation (σ'_h) of groundwater level ($h(x, t)$) versus the dimensionless time (t') at the dimensionless locations x'=0.0, 0.2, 0.4, 0.6, and 0.8. The graphs on the right~~

带格式的：居中

带格式的：居中，缩进：左侧： 0 厘米，悬挂缩进： 1.33 字符，首行缩进： -1.33 字符，定义网格后自动调整右缩进，行距：1.5 倍行距，到齐到网格

column (five graphs) are σ'_h versus x' for the different t': b) and d) are for t'= 0.0, 0.2, 0.4, 0.6 and 0.8, f) and h) are for t'=0.01, 0.1, and 1.0, and j) is for t'=0.01, 0.2, 0.4, 0.6 and 0.8. Also, a) and b) are based on Eq.(11) where $\sigma_W^2 = \sigma_Q^2 = \sigma_H^2 = 0$; c) and d) are based on Eq. (12) where $\sigma_{W_0}^2 = \sigma_Q^2 = \sigma_H^2 = 0$; e) and f) are based on Eq. (13) where $\sigma_{W_0}^2 = \sigma_W^2 = \sigma_H^2 = 0$; g) and h) are based on Eq. (14) where $\sigma_{W_0}^2 = \sigma_W^2 = \sigma_Q^2 = 0$; i) and j) are based on Eq.(15) where $\sigma_{W_0}^2 \neq \sigma_W^2 \neq \sigma_Q^2 \neq \sigma_H^2 \neq 0$.

Figure 3 The dimensionless power spectrum versus frequency (f) at the dimensionless locations x'=0.0, 0.2, 0.4, 0.6, 0.8, and 0.9. The graphs on the left column are for t_c= 40 day, the graphs on the middle column are for t_c = 400 day, and the graphs on the right column are for t_c = 4000 day. The graphs on the first row are the dimensionless spectrum S_{hh}/S_{QQ} when $S_{WW}=0$, $S_{HH}=0$, and $S_{QQ}\neq 0$ in Eq. (10), the graphs on the second row is S_{hh}/S_{HH} when $S_{WW}=0$, $S_{QQ}=0$, and $S_{HH}\neq 0$, the graphs on the third row are S_{hh}/S_{WW} when $S_{QQ}=0$, $S_{HH}=0$, and $S_{WW}\neq 0$, and the graphs on the bottom row is S_{hh}/S_{WW} when $S_{QQ}\neq 0$, $S_{HH}\neq 0$, and $S_{WW}\neq 0$

带格式的：字体：（中文） 黑体

带格式的：字体：（中文） 黑体

带格式的：字体：（中文） 黑体

带格式的：字体：（中文） 黑体

带格式的：字体：（中文） 黑体

带格式的：字体：（中文） 黑体

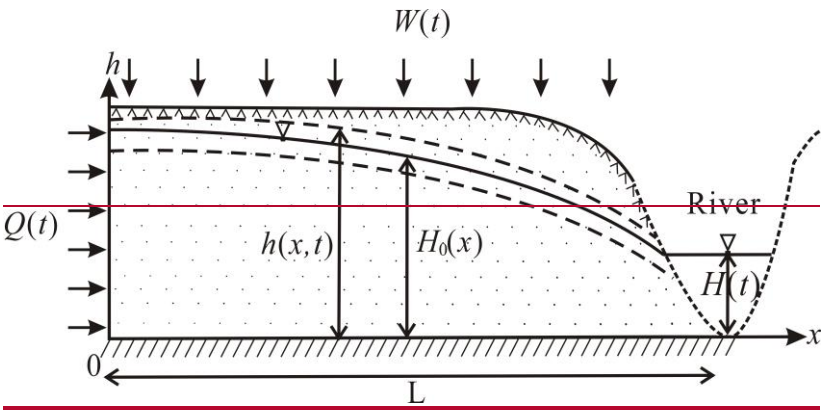

Figure 1 A schematic of the unconfined aquifer studied where W(t) is the time-dependent random source/sink, $H_0(x)$ is the random initial condition, Q(t) is the random time-dependent flux at the left boundary, H(t) is the random time-dependent water level at the right boundary, L [L] is distance from the left to the right boundary, and h(x, t) is the random groundwater level in the aquifer.

带格式的：居中

Figure 1 The standard deviation (σ'_h) of $h(x, t)$ versus the dimensionless time (t') at the dimensionless locations x'=0.0, 0.2, 0.4, 0.6, and 0.8 (the four graphs in the left column) and the standard deviation (σ'_h) of $h(x, t)$ versus the dimensionless location (x') for the dimensionless time t'=0.01, 0.1, and 1.0 (the four graphs in the right column): a) and b) are based on Eq.(11) where $\sigma_W^2 = \sigma_Q^2 = \sigma_H^2 = 0$; c) and d) are based on Eq. (12) where $\sigma_{W_0}^2 = \sigma_Q^2 = \sigma_H^2 = 0$; e) and f) are based on Eq. (13) where $\sigma_{W_0}^2 = \sigma_W^2 = \sigma_H^2 = 0$; g) and h) are based on Eq. (14) where $\sigma_{W_0}^2 = \sigma_W^2 = \sigma_Q^2 = 0$.

Figure 2 a) The standard deviation (σ'_h) of $h(x, t)$ versus the dimensionless time (t') at the dimensionless locations x'=0.0, 0.2, 0.4, 0.6, and 0.8 and b) the standard deviation (σ'_h) of $h(x, t)$ versus the dimensionless location (x') for the dimensionless time t'=0.01, 0.1, and 1.0, evaluated based on Eq.(15) where $\sigma_{W_0}^2 \neq \sigma_W^2 \neq \sigma_Q^2 \neq \sigma_H^2 \neq 0$.

Figure 3 The dimensionless power spectrum versus frequency (f) at the dimensionless locations x'=0.0, 0.2, 0.4, 0.6, 0.8, and 0.9. The left column is for t_e = 40 day, the middle column is for t_e = 400 day, and the right column is for t_e = 4000 day. The first row is the dimensionless spectrum S_{hh}/S_{QQ} when $S_{WW} = 0$, $S_{HH} = 0$, and $S_{QQ} \neq 0$ in Eq. (10), the second row is S_{hh}/S_{HH} when $S_{WW} = 0$, $S_{QQ} = 0$, and $S_{HH} \neq 0$, and the bottom row is S_{hh}/S_{WW} when $S_{QQ} = 0$, $S_{HH} = 0$, and $S_{WW} \neq 0$.

Figure 4 The dimensionless power spectrum versus frequency (f) at the dimensionless locations x'=0.0, 0.2, 0.4, 0.6, 0.8, and 0.9 when $S_{QQ} \neq 0$, $S_{HH} \neq 0$, and $S_{WW} \neq 0$ for a)

带格式的: 居中, 缩进: 左侧: 0 厘米, 悬挂缩进: 1.33 字符, 首行缩进: -1.33 字符, 定义网格后自动调整右缩进, 行距: 1.5 倍行距, 到齐到网格

t_c = 40 day, b) t_c = 400 day, and c) t_c = 4000 day.

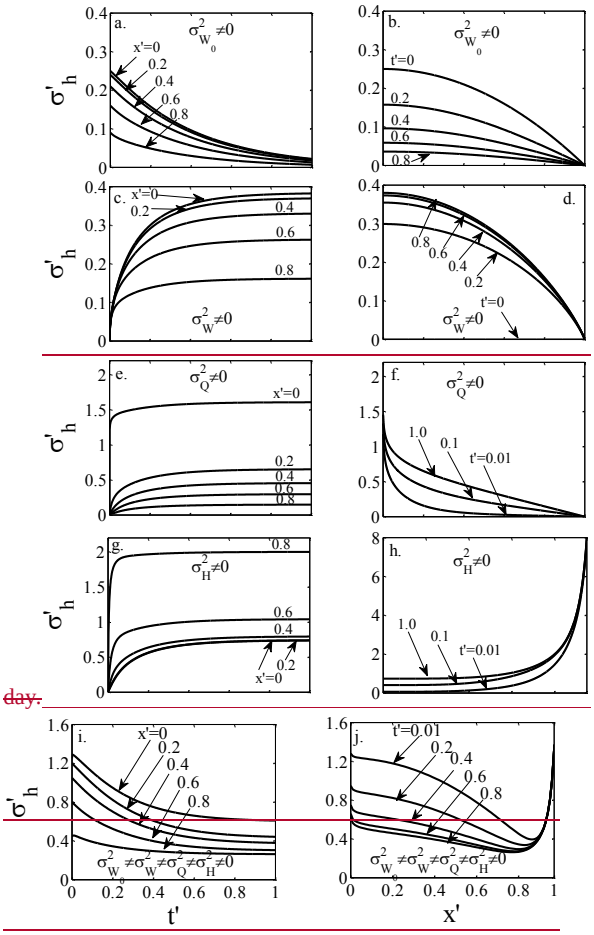

Figure 2 The graphs on the left column (five graphs) are the standard deviation (σ'_h) of groundwater level ($h(x, t)$) versus the dimensionless time (t') at the dimensionless locations x'=0.0, 0.2, 0.4, 0.6, and 0.8. The graphs on the right column (five graphs) are σ'_h versus x' for the different t': b) and d) are for t'= 0.0, 0.2, 0.4, 0.6 and 0.8, f) and h) are for t'=0.01, 0.1, and 1.0, and j) is for t'=0.01, 0.2, 0.4, 0.6 and 0.8. Also, a) and b) are based on Eq.(11) where $\sigma^2_W = \sigma^2_Q = \sigma^2_H = 0$; c) and d) are based on Eq. (12) where $\sigma^2_{W_0} = \sigma^2_Q = \sigma^2_H = 0$;

e) and f) are based on Eq. (13) where $\sigma_{W_0}^2 = \sigma_W^2 = \sigma_H^2 = 0$; g) and h) are based on Eq. (14) where $\sigma_{W_0}^2 = \sigma_W^2 = \sigma_Q^2 = 0$; i) and j) are based on Eq.(15) where $\sigma_{W_0}^2 \neq \sigma_W^2 \neq \sigma_Q^2 \neq \sigma_H^2 \neq 0$.

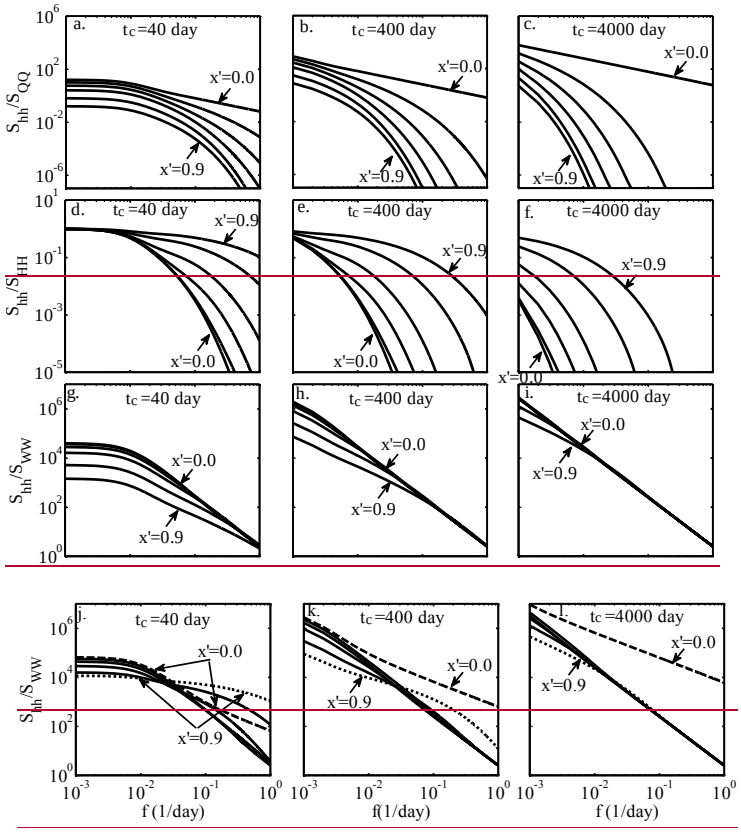

Figure 3 The dimensionless power spectrum versus frequency (f) at the dimensionless locations x'=0.0, 0.2, 0.4, 0.6, 0.8, and 0.9. The graphs on the left column are for t_c = 40 day, the graphs on the middle column are for t_c = 400 day, and the graphs on the right column are for t_c = 4000 day. The graphs on the first row are the dimensionless spectrum S_{hh}/S_{QQ} when $S_{WW} = 0$, $S_{HH} = 0$, and $S_{QQ} \neq 0$ in Eq. (10), the graphs on the second row is S_{hh}/S_{HH} when $S_{WW} = 0$, $S_{QQ} = 0$, and $S_{HH} \neq 0$, the graphs on the third row

带格式的：字体：（中文）黑体

611 ~~are S_{hh}/S_{WW} when $S_{QQ}=0$, $S_{HH}=0$, and $S_{WW}\neq 0$, and the graphs on the bottom row is~~

612 ~~S_{hh}/S_{WW} when $S_{QQ}\neq 0$, $S_{HH}\neq 0$, and $S_{WW}\neq 0$,~~

613

带格式的：字体：（中文） 黑体

带格式的：字体：（中文） 黑体

带格式的：字体：（中文） 黑体

带格式的：字体：（中文） 黑体

带格式的：字体：（中文） 黑体

带格式的：字体：（中文） 黑体